

10. TURBIDITE SEDIMENTOLOGY AND HISTORY OF THE EAST MARIANA BASIN¹

Jill M. Whitman, Geological Research Division, Scripps Institution of Oceanography
Miriam Baltuck, Department of Geological Sciences, Tulane University
Janet A. Haggerty, Department of Geosciences, University of Tulsa
and

Walter Dean, U.S. Geological Survey, Denver²

ABSTRACT

At Site 585 in the East Mariana Basin, a 900-m section of Aptian–Albian to Recent sediments was recovered. The upper 590 m are pelagic components (carbonate, siliceous, and clay); small-scale graded sequences and laminations are common. The underlying sediments are volcanoclastic sandstones with a large proportion of shallow-water carbonate debris; sedimentary structures including complete Bouma sequences, cross-laminae, and scouring are common. These structures indicate that the entire section was deposited by turbidity currents. The change in lithology upward in the section reflects the evolution of the surrounding seamounts, from their growth stages during the middle of the Cretaceous to the later subsidence phases. Several black layers containing pyritized organic debris and associated turbidite structures were cored near the Cenomanian/Turonian boundary; this material has been transported from the flanks of the seamounts where it was deposited within a shallow anoxic zone. Seismic data extends the stratigraphy across the entire Basin, showing the reflectors onlapping the seamounts, and indicating at least 1200 m of sediment at Site 585. The crust is placed at 6900 m after correcting for sediment loading, and the subsidence curve indicates that the Basin has been deeper than 5500 m since before the Aptian.

INTRODUCTION

Site 585 was drilled in the East Mariana Basin at a water depth of about 6100 m. This Basin is encircled by the Caroline Seamounts and the Magellan Seamounts (Fig. 1). The crust at this site is Jurassic in age, on the basis of its depth and the extrapolation of spreading rates from Mesozoic magnetic anomalies (Shipley et al., 1983).

One of the significant aspects of the sediments drilled at Site 585 is the extent of resedimented material throughout the entire section. There is a marked change in the sediments from basal volcanoclastic-rich turbidite sands up to turbidites of partially winnowed pelagic components interbedded with zeolitic claystone. This sequence records the growth and subsidence history of the Basin and the numerous seamounts that surround it.

In this chapter we present a sedimentologic description of the turbidites. Petrographic and petrologic aspects are treated in greater detail elsewhere in this volume (Baltuck; Floyd; Haggerty and Premoli Silva). Our discussion includes evaluations of both the gross morphologic changes between the units and the finer-scale changes within the basal volcanoclastic unit. We also present an interpretation of the sedimentation history with particular emphasis placed on the subsidence history of the Basin and the nearby volcanic edifices.

SITE 585 SEDIMENTS

Lithologies Drilled at Site 585

Two holes were drilled at Site 585. The first hole (585) was washed to 256 m after one core was collected at the sediment/water interface and then cored continuously until drilling was impeded at 764 m. The second hole (585A) was spot-cored in a few intervals of interest (Cretaceous/Tertiary boundary, the Cenomanian/Turonian boundary), then cored continuously below 772 m until bit failure at 893 m.

The sediments recovered at this site are divided into six units on the basis of composition and degree of diagenesis and lithification (Table 1). The upper five units (I–V) are composed primarily of pelagic components with varying proportions of carbonate, siliceous debris, and clay. The sediments are generally fine clays and silty clays, with radiolarian-rich sandy layers occurring primarily in Unit V. Unit VI is composed of volcanoclastic material with grain sizes ranging from clay to cobble-sized clasts.

Evidence for sediment reworking exists throughout the section. Diagnostic features include the occurrence of shallow-water carbonate material, the discordant ages of microfossils, internal sedimentary structures, and high sedimentation rates.

Shallow-water carbonate material is common in the lower third of the section (590–893 m); this debris includes benthic foraminifers, echinoid fragments and spines, rare algal fragments, sponge spicules, bryozoans, rudist fragments, and ooids. Fauna typically associated with reefal environments, such as rudist fragments and abundant algal debris, are rare.

Sedimentary structures indicative of resedimentation include partial or complete Bouma sequences, basal scour,

¹ Moberly, R., Schlanger, S. O., et al., *Init. Repts. DSDP*, 89: Washington (U.S. Govt. Printing Office).

² Addresses: (Whitman) Geological Research Division, A-008, Scripps Institution of Oceanography, University of California, San Diego, La Jolla, CA 92093; (Baltuck) Dept. of Geological Sciences, Tulane University, New Orleans, LA 70118; (Haggerty) Dept. of Geosciences, University of Tulsa, 600 S. College Ave., Tulsa, OK 74104; (Dean) U.S. Geological Survey, Box 25046, MS 940, Denver Federal Building, Denver, CO 80225.

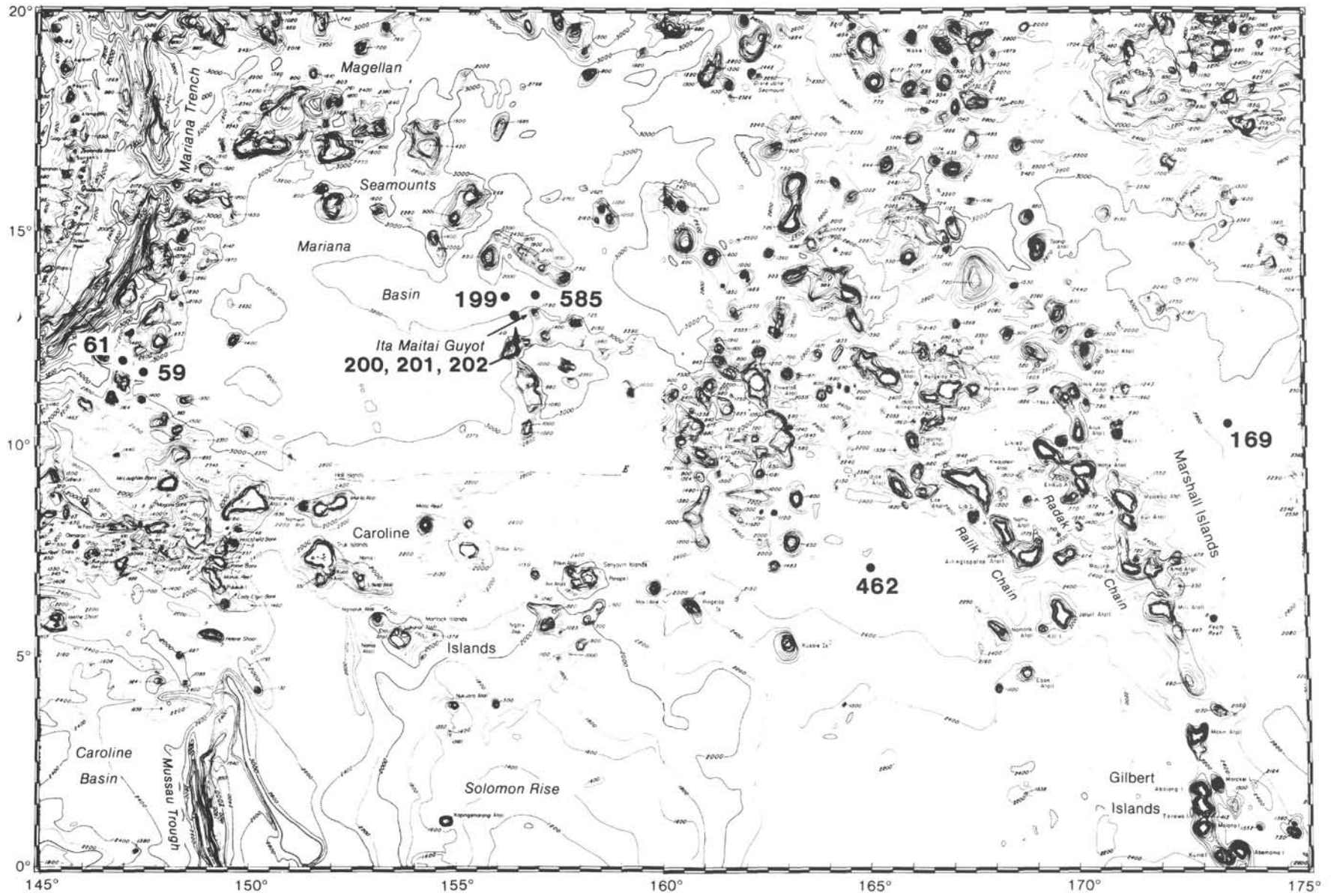


Figure 1. Regional bathymetry of the western Pacific with locations of DSDP sites indicated. (after Chase et al., 1970, 1971; depths are in fathoms).

Table 1. Lithologic units at Site 585.

Unit	Lithology	Cores (hole-core range)	Sub-bottom depth (m)	Thickness (m)	Age
I	Nannofossil ooze, clay-bearing nannofossil ooze, and clay	585-1	0-6.8	6.8	Recent to lower Pleistocene
II	Nannofossil chalk, silicified limestone, chert, and zeolitic claystone	585-2-17 585A-1-3	256-399	143	Middle Miocene to Maestrichtian
III	Zeolitic claystone, nannofossil claystone, and clayey nannofossil chalk and chert	585-18-20	399-426	27	Maestrichtian to upper Campanian
IV	Chert and claystone	585-21-26 585A-4	426-485	59	Campanian
VA	Brown and olive black claystone	585-27-28	485-504	19	Campanian
VB	Dark gray claystone	585-29-23 585A-5-9	504-550	46	Coniacian to upper Cenomanian
VC	Calcareous claystone, radiolarian claystone, and clayey limestone	585-34-37 585A-9,CC-10	550-590	40	Cenomanian to middle Albian
VI	Graded sequences of volcanic sandstones, siltstones, and claystones	585-38-55 585A-11-22	590-893	303	Middle Albian to upper Aptian

and graded bedding. The accumulation of carbonate material at depths far below the calcite compensation depth (CCD) also suggests transport from a shallower source and rapid burial.

Unit I (585-1; 0-6.8 m sub-bottom)

Unit I represents the upper 6.8 m of sediments at this site. The sediments of Unit I are Recent and Pleistocene in age, with 1.5 m of brown clay overlying 5 m of nannofossil ooze. The carbonate ooze was deposited at a depth of about 6100 m in a region where the CCD is at about 4500 m (Berger and Winterer, 1974), which strongly suggests that the sediments were redeposited.

Unit II (585-2-17, 585A-1-3; 256-399 m sub-bottom)

Unit II contains middle Miocene to Maestrichtian nannofossil chalk, silicified limestone, chert, and zeolitic claystone. The abundant chert and silicified limestone inhibited coring, and recovery for the entire unit averaged less than 18%. No sedimentary structures were observed, and the softer lithologies interbedded with the cherts were not recovered. Claystone beds range in thickness from 10 to 60 cm, and the nannofossil-rich layers reach thicknesses of greater than 3 m. The presence of nannofossil chalk again suggests that carbonate material was transported into the Basin from a shallow site of initial accumulation.

Unit III (585-18-20; 399-426 m sub-bottom)

The sediments of Unit III consist of Maestrichtian to upper Campanian zeolitic claystone, nannofossil claystone, and minor nannofossil chalk and chert. Claystone dominates this unit, layered with varying amounts of CaCO₃ as nannofossils and unspecified carbonate, but there is less carbonate material than in Unit II. Subtle grading is observed in the thin laminae near the bases of carbonate-rich beds. The laminae contain silt-sized ashy material and grade up into zeolite-bearing calcareous claystone.

Unit IV (585-21-26, 585A-4; 426-485 m sub-bottom)

Unit IV (Campanian) had the lowest recovery of all the units (averaging about 3%), with the sediments consisting of chert and claystone. There is obvious layering in some of the larger chert fragments. Microscopic examination reveals that these cherts formed from silicification of graded carbonate grainstones (Baltuck, this volume).

Unit V (585-27-37, 585A-5-10; 485-590 m sub-bottom)

Campanian to middle Albian sediments were recovered in Unit V. The dominant lithology is claystone. Varying proportions of zeolites, carbonate material, and radiolarian sandstones were used to subdivide the unit into three subunits. Laminations and graded beds are common in each of the three subunits.

Subunit VA (485-504 m) is composed of Campanian dark reddish brown and olive black zeolite-bearing claystone. Most samples contain less than 10% silt (zeolite, feldspar, volcanic glass, and iron oxide). Light green silty laminations are common, and some of these layers appear to form the bases of graded sequences.

The Coniacian to upper Cenomanian Subunit VB (504-550 m) is composed of dark gray claystone with variable amounts of calcareous, siliceous, and organic material. Laminations, graded intervals, and discrete layers or lenses of sand can be distinguished. The sand-sized component consists primarily of recrystallized radiolarians. In many cases, the sand layers form the bases of fining-upward sequences, some of which exceed 3 m in thickness.

Four thin black layers are present near the Cenomanian/Turonian boundary. Two layers have high concentrations of organic carbon (up to 9.9%), whereas the other two layers are not rich in organic carbon (Site 585 report, this volume). The uppermost layer of organic matter occurs at the silty base of a turbidite (Fig. 2). The organic-carbon content of this black layer is about 0.25%.

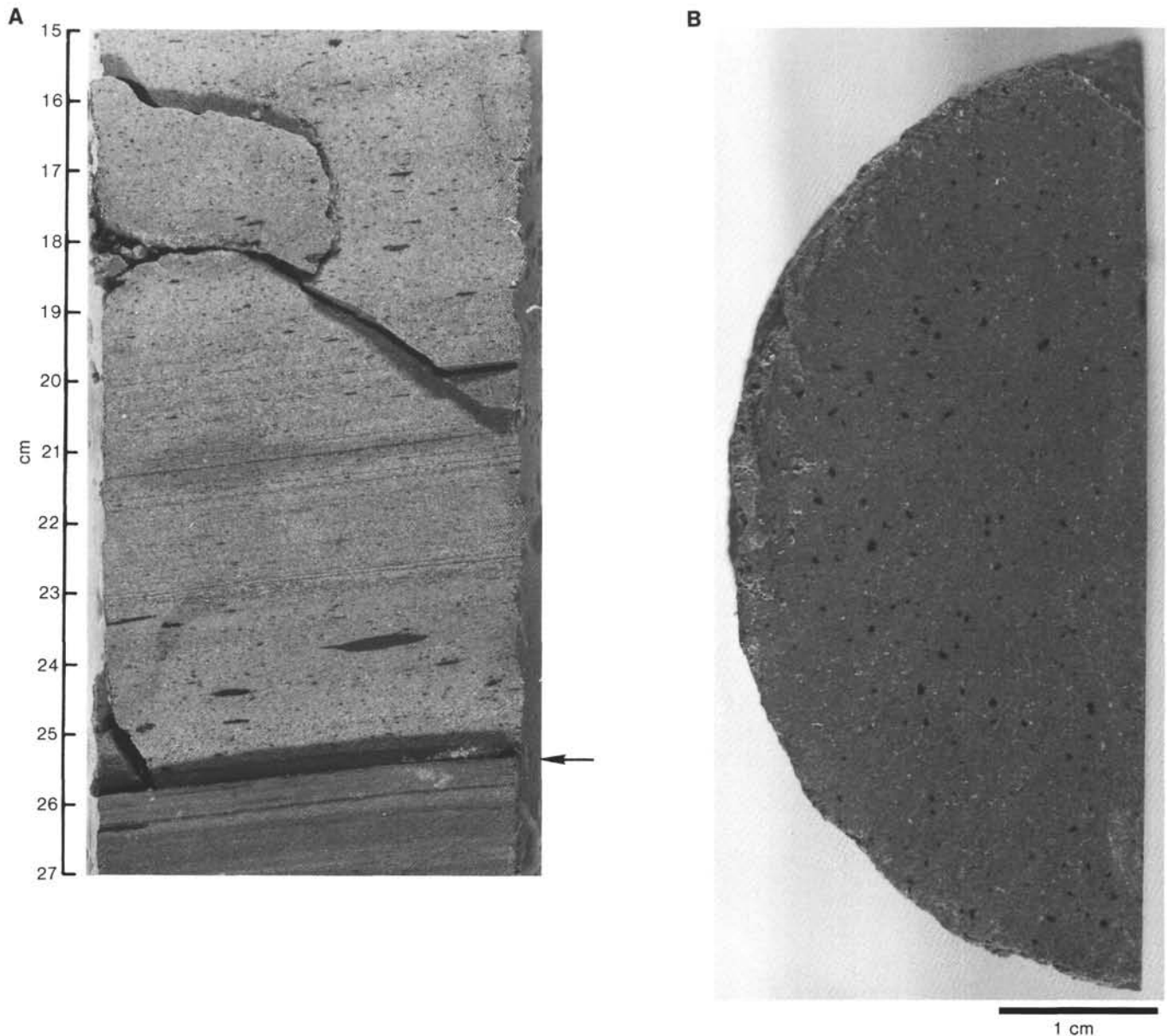


Figure 2. A. Radiolarian-rich silty claystone turbidite in Subunit VB (Sample 585-32-3, 15–27 cm, 534.4 m sub-bottom depth) showing basal 2-mm-thick, organic carbon-rich layer (at 25 cm). Pyrite flecks up to 1 cm long occur in fining-upward sequence over a 3-m interval (Samples 585-32-1, 0 cm to 585-32-3, 25 cm). B. Same turbidite, sampled slightly upsection (Sample 585-32-1, 104 cm) of the interval in 2A. Core is cut parallel to stratification, showing pyrite flecks in plane of deposition. Bar scale = 1 cm.

Flecks of organics are oriented parallel to stratification, and the size and abundance of the flecks increase downward over a distance of about 3 m to a 2-mm-thick black layer. The bottom few centimeters of this turbidite are laminated, and the laminations contain recrystallized radiolarians, organic debris, and rare benthic foraminifers mixed with clay (Fig. 3). The organic debris is partially pyritized, which probably had occurred prior to transport by the turbidity current. If this organic material had been pyritized after deposition, the particles would not have responded as a higher-density component with the siltstone.

The second black layer containing 5.4% organic carbon also occurs at the base of a turbidite. The upper di-

vision of this turbidite is a burrowed dark gray claystone. The sequence grades downward through silt-bearing claystone containing black flecks of organic matter to a dark gray silty claystone containing radiolarians and foraminifers. The base of the turbidite is distinguished by parallel laminations and cross-laminations (Fig. 4), containing divisions B–E of the Bouma sequence (Middleton and Hampton, 1973).

The other two black layers were recovered in Hole 585A. The third layer is in a silty claystone containing recrystallized radiolarians; the organic-carbon content of the black layer is 1.45%. The bed forms the base of a fining-upward sequence peppered with black flecks that continues throughout Core 585A-8.

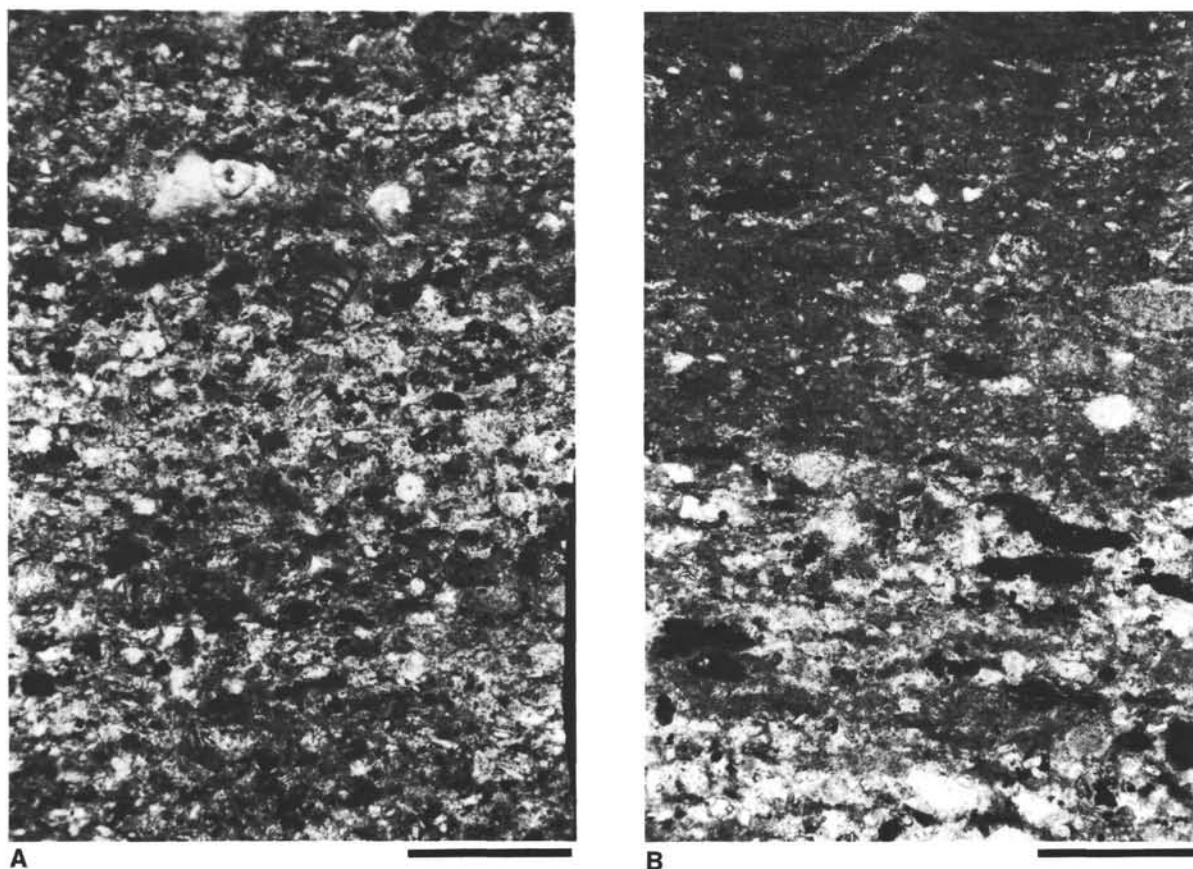


Figure 3. Photomicrographs from base of organic carbon-rich turbidite deposit, Sample 585-32-3, 20–23 cm. Bar scale = 0.5 mm. A. Basal portion of deposit contains abundant recrystallized radiolarians, organic detritus, and rare benthic foraminifers mixed with clay. The clay content varies, which gives the appearance of layering. B. Area of sample immediately overlying the location shown in 3A. Note the distinct change to a more clay-rich portion of the turbidite. The large clasts of organic detritus are elongated and aligned parallel to the laminations in the silty claystone as well as in the claystone.

The last of the black layers has a very different lithologic association from the others recovered at this site. The 4-mm-thick black band contains less than 0.1% organic carbon and occurs within a fragment of laminated radiolarian-bearing siltstone. The siltstone is overlain by fragments of brightly colored red, brown, and yellow chert containing flecks and lenses of pyrite up to 1 mm in largest visible dimension. The layer is not graded, and the concentration of material in the black band may have been produced by the chertification process.

Subunit VC (550–590 m) is composed of Campanian to middle Albian claystone with variable concentrations of carbonate material and radiolarians. Grain size varies considerably within this subunit, and laminated beds containing over 50% sand are common throughout the interval (Fig. 5). The darker basal layers in several beds are formed by concentrations of radiolarians.

In summary, the sediments of Units I through V contain primarily redeposited pelagic components. Small-scale graded sequences and laminations are common and increase in frequency toward the base of the section. The bases of the graded sequences are concentrated in volcanoclastic debris and radiolarians. Radiolarian-rich turbidites are particularly common in Unit V, and organic-carbon-rich layers are unique to Subunit VB.

Volcanoclastic Turbidites—Unit VI

Unit VI (middle Albian to upper Aptian, 590–893 m sub-bottom) contains volcanoclastic sandstone, dominated by hyaloclastic debris in various shades of green. The clast types include altered volcanic glass, volcanic lithic and crystalline fragments (feldspar, olivine, clinopyroxene, and other heavy minerals), celadonite, and zeolites (Floyd, this volume).

Some beds of Unit VI contain large amounts of carbonate debris or mixed carbonate and volcanoclastic material. The carbonate component of these beds is dominated by shallow-water debris, which includes ooids, benthic foraminifers, algae, bryozoans, and rudist fragments (Haggerty and Premoli Silva, this volume). Some contribution from pelagic microfossils is also apparent. The concentration of the shallow-water carbonate components at the base of these turbidite deposits is due almost entirely to the coarser grain size and greater density of the carbonate clasts.

Turbidites dominated by carbonate debris are more common in the upper part of Unit VI, whereas below Core 52 (732 m sub-bottom), the turbidites contain mostly volcanoclastic material. Figure 6A displays coarse-tail grading within Bouma division A of a carbonate-rich turbidite.

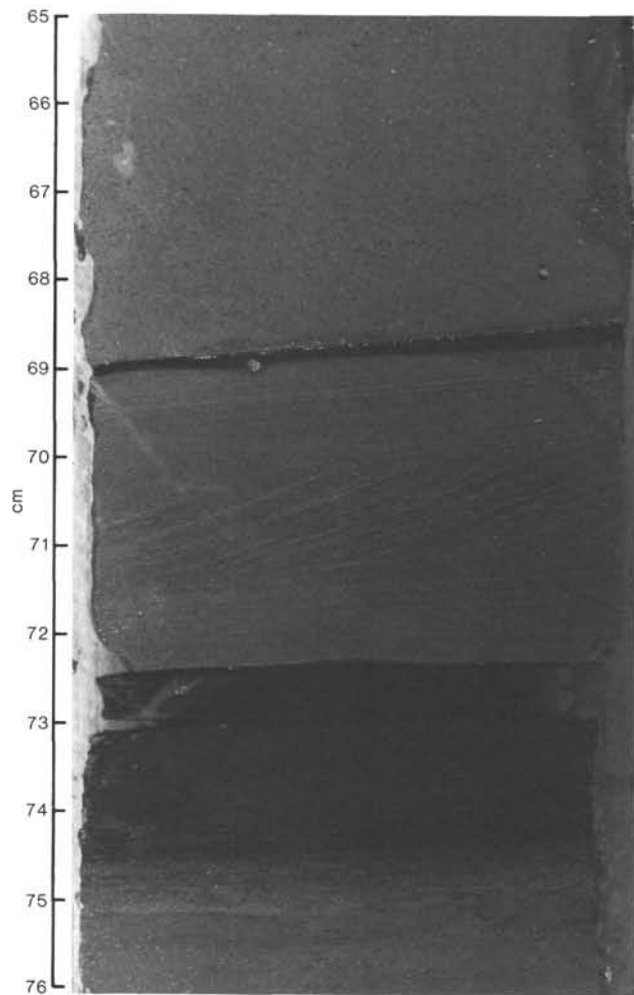


Figure 4. Organic carbon-rich turbidite in Subunit VB (585-32-3, 65–76 cm) with parallel laminations and cross-laminations in the interval 69–73 cm overlying the 2-cm-thick organic carbon-rich pyritic black layer of silty claystone at 72–74 cm (534.9 m sub-bottom depth).

dite; the coarser-grained sediment in this example is primarily ooids and skeletal debris within a mud matrix (Fig. 6B). More typically, the basal Bouma division A contains little mud matrix (Fig. 6C). Opaque and heavy minerals that are concentrated in Bouma division A are also found at the bottoms of ripples and wavy laminations in division C.

A great range of grain sizes is represented by the sediments of Unit VI. The turbidites of the upper portion contain coarse sandstone and conglomeratic sandstone. The lowermost beds (838–893 m sub-bottom, Cores 585A-16 to -22) are poorly sorted, and clast size ranges up to cobble. This portion of the unit is interpreted as debris-flow deposits (Site 585 report, this volume).

Sedimentary structures, including complete and incomplete Bouma sequences (Figs. 7 and 8), cross-laminae (Fig. 9), scouring (Figs. 8, 9, and 10), and load casts (Figs. 11 and 12) are common. The tops of many of the turbidites grade upward into the pelitic Bouma division E with clay of various colors ranging from reddish brown to very dark gray to light greenish gray. Some of the

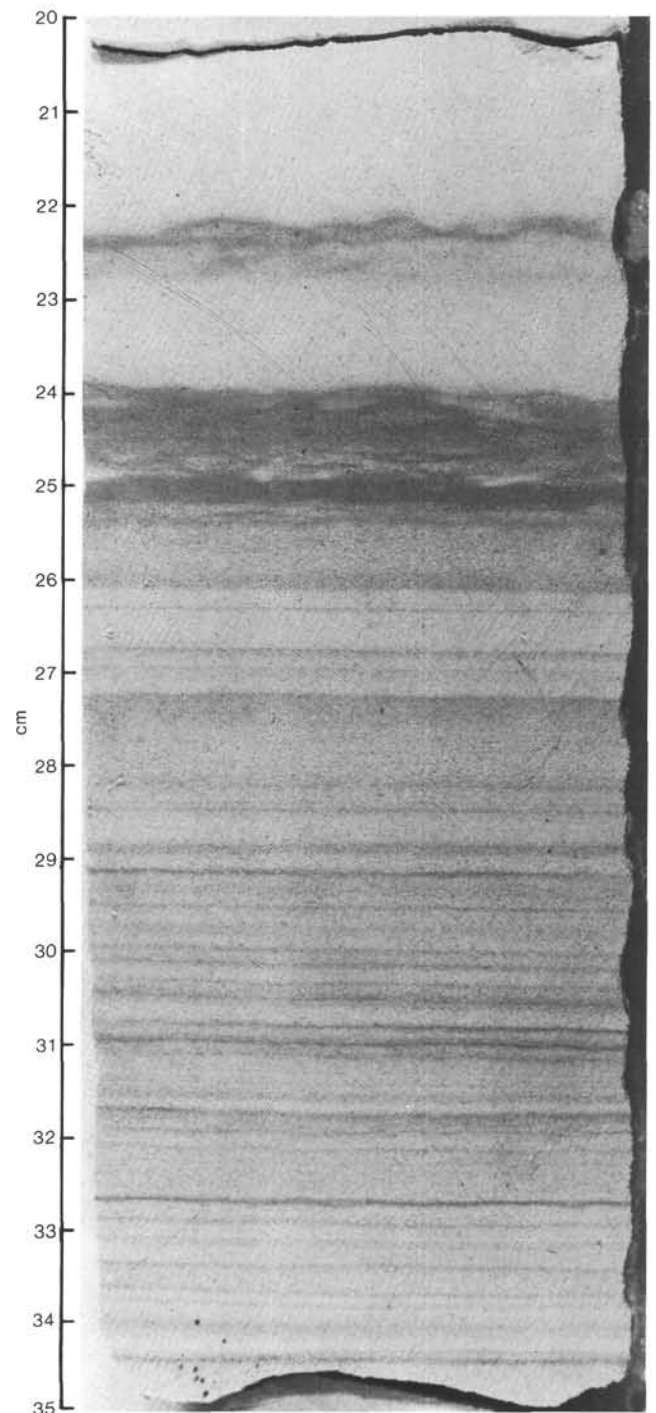


Figure 5. Thinly laminated nannofossil-bearing limestone of Subunit VC (585-34-2, 20–35 cm). Dark layers are formed by concentrations of radiolarians. (Sampled at a sub-bottom depth near 550 m.)

claystone has a significant proportion of carbonate material (unspecified carbonate and nannofossils) and there is abundant evidence of bioturbation. The burrows are commonly distinguished by sediment fill different from that which surrounds them or by differential cementation. Thickness of the pelitic intervals reaches a maximum of 150 cm and bioturbation is better developed in thicker pelitic divisions (Figs. 7 and 10).

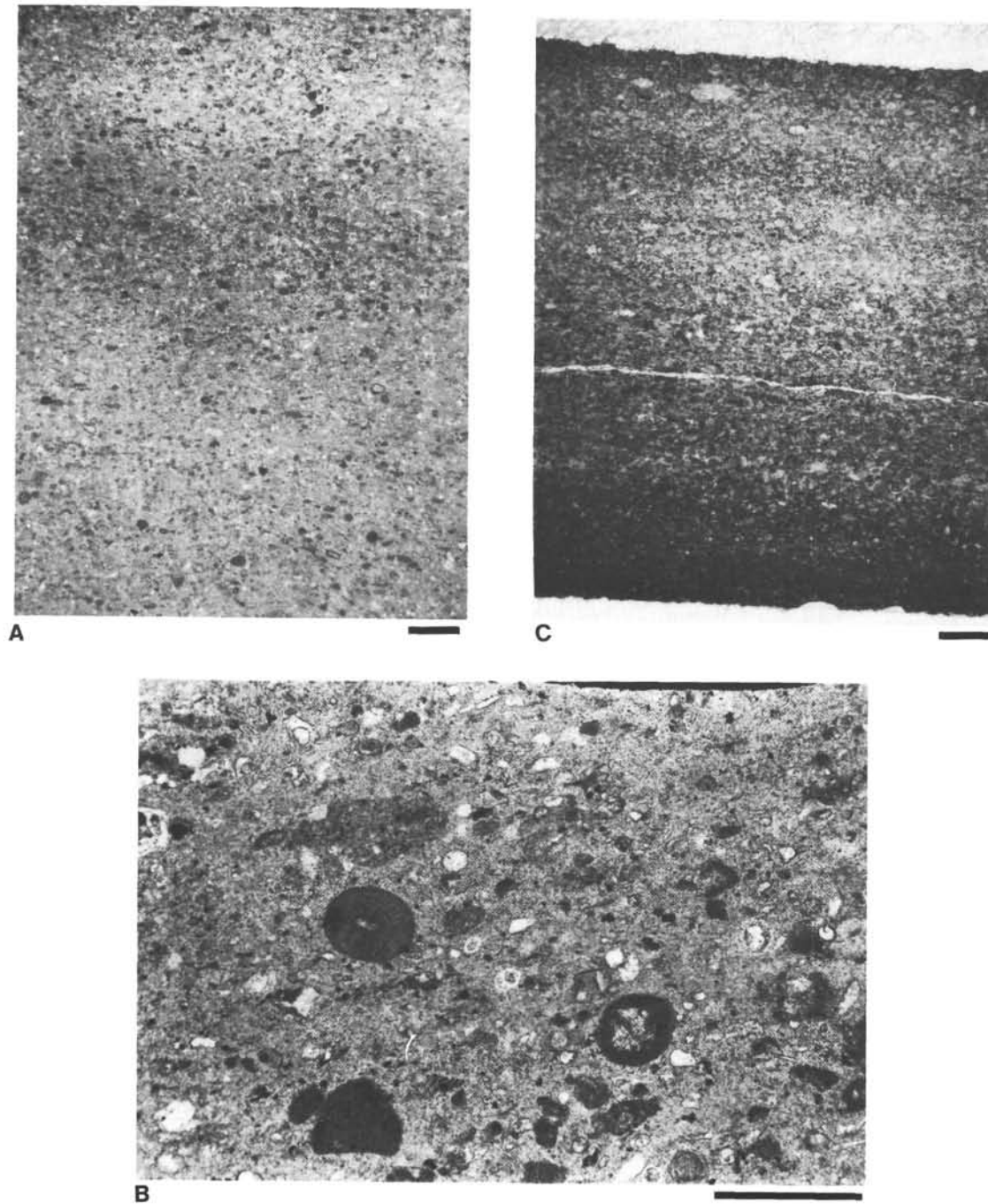


Figure 6. A. Photomicrograph of Sample 585-38-1, 45–50 cm displays coarse-tail grading within Bouma division A. (Plane polarized light; bar scale = 2.0 mm.) B. Photomicrograph of same sample as in 6A. The coarser-grained sediment is primarily ooids and skeletal debris in a mud matrix. (Plane polarized light; bar scale = 0.5 mm.) C. Photomicrograph of Sample 585-43-2, 58–60 cm. Typical basal Bouma division A of carbonate-rich turbidite deposits with little mud matrix. (Plane polarized light; bar scale = 2.0 mm.)

Many of the coarser volcanoclastic sandstones at the bases of turbidites contain clasts up to a few centimeters in diameter. Clast types include basalt, claystone, volcanic glass, and shallow-water carbonate debris (Figs. 13 and 14).

In summary, thick, middle Albian–upper Aptian turbidites are abundant between 590 and 893 m sub-bottom depth, and sedimentary structures are indicative of scouring and high velocities of transport. The thickness of the section demonstrates that large volumes of mate-

rial were produced largely through volcanic processes, then transported and redeposited in the Mariana Basin.

Turbidite Thicknesses

The thicknesses of the turbidites in Unit VI vary from 2 cm to almost 400 cm (Core 52, Hole 585). The average recovery in this unit was 57%. In general, the carbonate turbidites are thinner (less than 30 cm), whereas thicker turbidites are composed of volcanoclastic debris. In relative terms, thinner turbidites are present throughout the

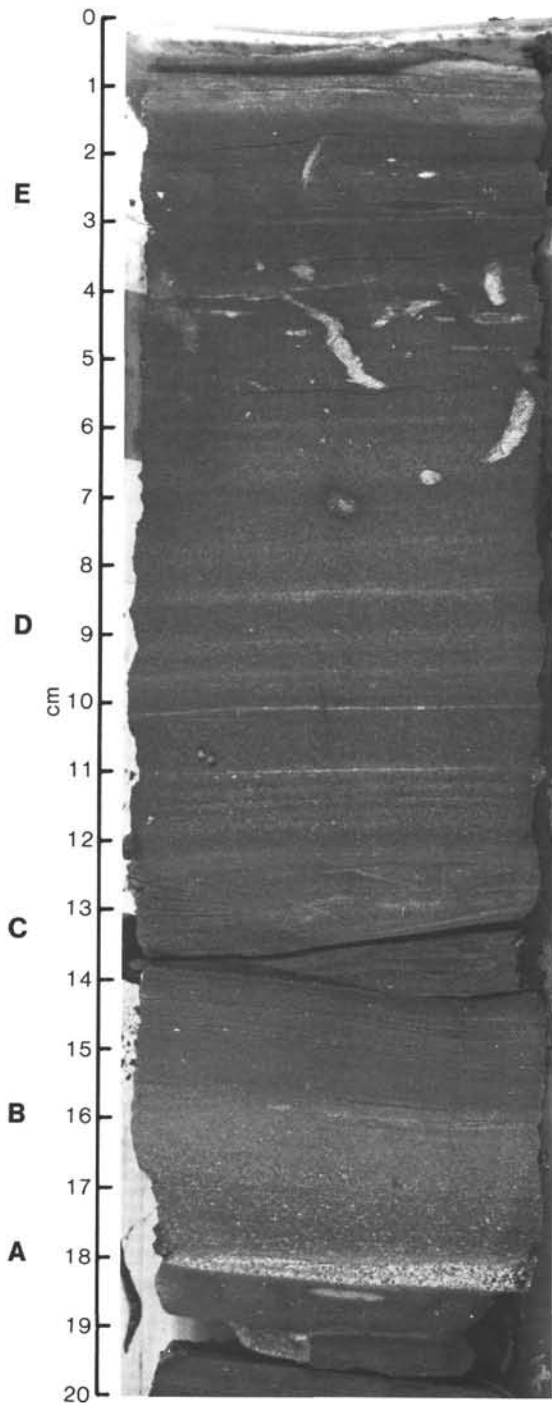


Figure 7. Carbonate-rich volcaniclastic turbidite with all Bouma divisions (A-E) present (585-39, CC [0-20 cm], Unit VI). Bioturbation present in interval 2-7 cm (Bouma division A). Cross bedding in interval 12-15 cm (Bouma division C).

unit, but the abundance of thicker turbidites increases with depth (Figs. 15 and 16; Table 2). This is particularly obvious in the distribution of individual turbidites greater than 50 cm; this thickness appears to be an average cut-off between the few very thick turbidites and the more common "background thickness" (Fig. 15). The occurrence of very thick turbidites (>150 cm) is scattered below a sub-bottom depth of 640 m, showing a

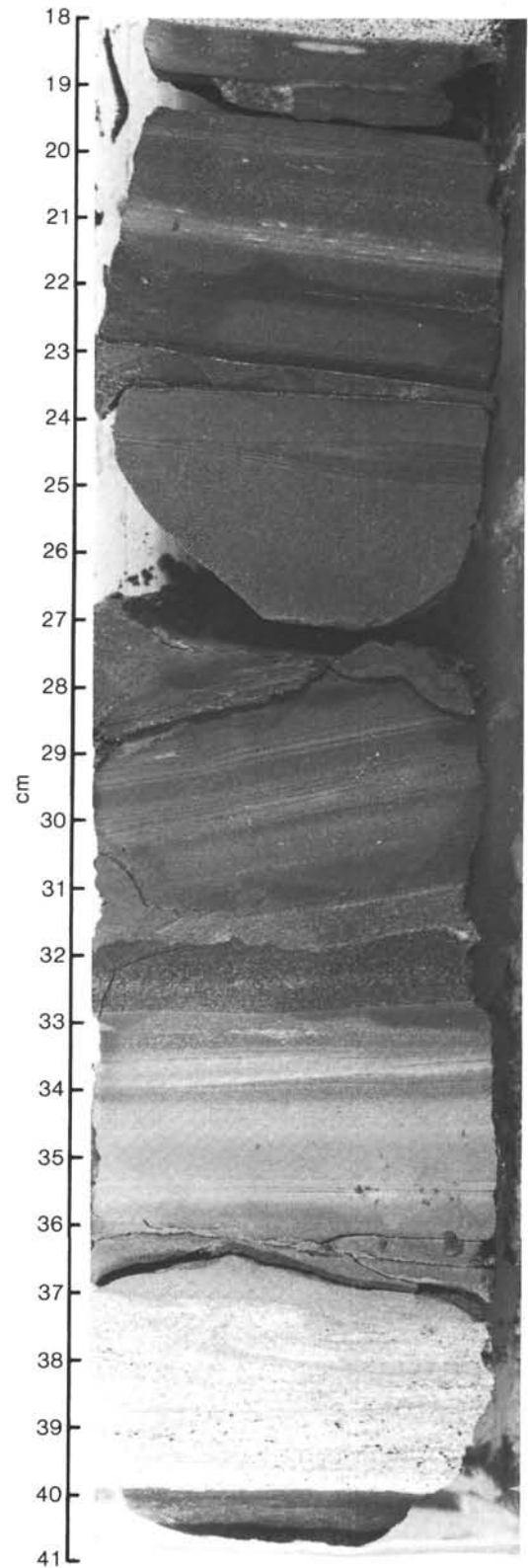


Figure 8. Truncated sequences of carbonate-rich sandstones and siltstones in Unit VI (585-39, CC [20-41 cm]). Note scoured surfaces at 32 and 33 cm.

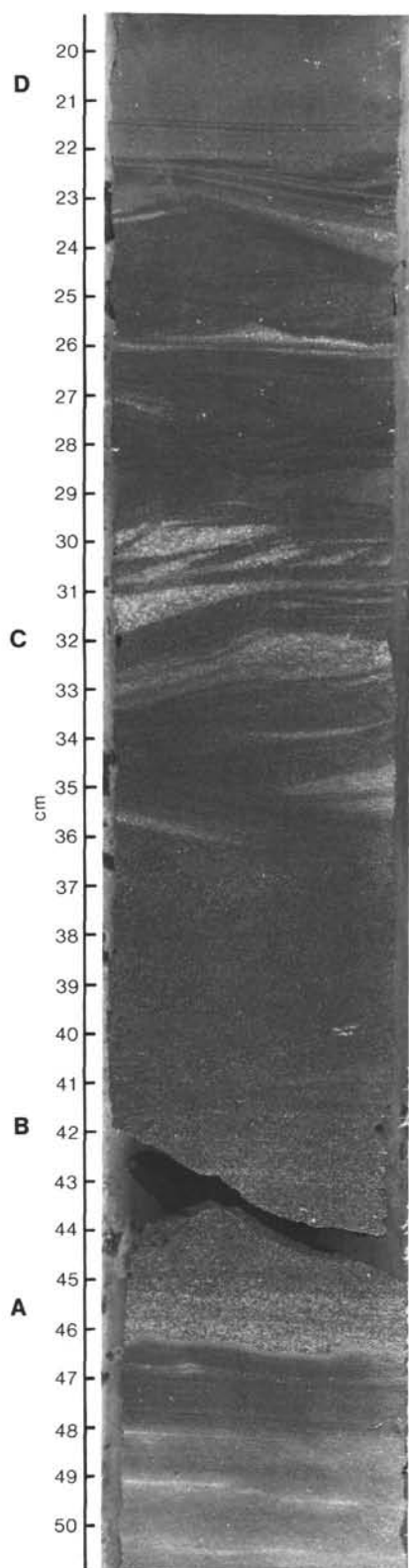


Figure 9. This core from Unit IV (585A-H5-5, 20-50 cm) contains a particularly thick interval (22-36 cm) of cross-bedding in carbonate-rich volcanoclastic sandstone. The transition from the upper-flow regime (graded division [A] and lower division of parallel lamination [B]) to the lower-flow regime (division of current ripple lamination [C] and upper division of parallel lamination [D]) is well illustrated. Note scoured base at 47 cm.

slight increase in frequency with depth. The peak in turbidite thickness occurs in the interval from 710 to 730 m sub-bottom (Cores 51 and 52), where two layers of thickness greater than 350 cm were recovered. Both of these turbidites are graded from coarse volcanoclastic sandstones up to burrowed claystones, with intervals dominated by laminations in silty claystone.

ORIGIN OF THE TURBIDITES

Seamounts have played a major role in the history of sedimentation in the East Mariana Basin. The Basin is bordered by the Caroline Seamounts to the south and the Magellan Seamounts to the north (Figure 1). The sediments of Unit VI record a growth phase of the seamounts surrounding Site 585. The hyaloclastic debris in this unit was produced by the explosive interaction between magma and seawater, which shows that the eruption of this material occurred close to sea level. Debris flows in the lower part of the unit contain large basalt clasts, suggesting a rapid growth phase of the seamounts. Large amounts of debris accumulated on the volcanic edifices and were redeposited into the Basin. The thick, well-developed turbidites above the debris-flow deposits contain primarily hyaloclastic debris. Turbidite thickness decreases in the uppermost part of this unit, suggesting that the volume and rate of supply of the material may have decreased. Sedimentation rates of Unit VI are high, at least 40 m/m.y. (Fig. 17); this rapid rate of supply probably corresponds to a major growth phase of the seamounts.

Deposition of Unit VI took place during the late Aptian to middle Albian (Site 585 report, this volume) over a maximum of 9 m.y. We studied the sedimentation rate of the pelitic division of Unit VI turbidites and dividing the total by 9 m.y. Placement of the boundary between divisions D and E was based on visual core descriptions corroborated where possible by shipboard smear-slide analyses; division E was restricted to sediment containing a clay fraction > 88%. The sedimentation rate so obtained is 2.2 m/m.y., more than twice that of pelagic red clay (Bouma and Hollister, 1973). Thus we conclude that the pelitic division of Unit VI contains a significant admixture of transported material.

The number of turbidites in the recovered section is 415, which corresponds to an average of about 22 thousand years between turbidity current flows. However, the numerous scoured basal contacts and missing upper divisions of turbidite sequences demonstrate the erosive nature of the turbidity flows, which could increase the apparent length of time between flows.

Shallow-water carbonate debris recovered throughout the unit includes ooids and biogenic debris from foraminifers, echinoids, bryozoans, rudists, and shallow-water algae. The presence of ooids indicates a source that was very close to sea level. The admixture of ooids in the volcanoclastic sediments suggests that the volcanic sources were topped with shallow-water carbonate deposits. At Site 202, drilled on Ita Maitai Guyot south of Site 585 (Fig. 1), a 30- to 40-m-thick layer of oolitic limestone older than middle Eocene was recovered (Heezen, Mac-

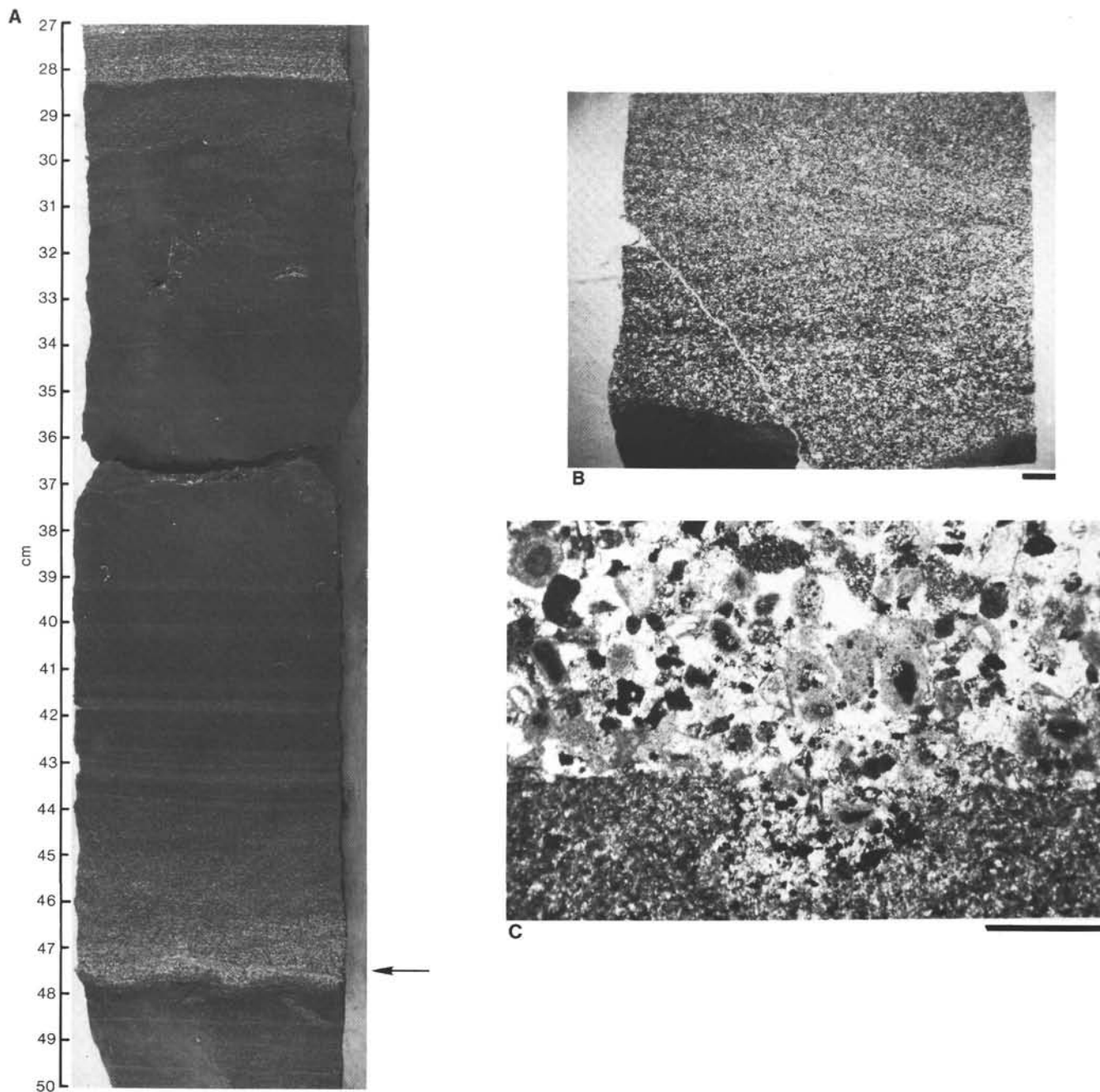


Figure 10. A. Unit VI volcanoclastic turbidite (585-54-3, 27-50 cm) with scoured base (at 47 cm). Note parallel laminations beneath scoured base suggesting that the underlying turbidite was truncated. B. Photomicrograph of Sample 585-54-3, 47-49 cm showing small-scale groove cutting into the underlying sediment. These sediment particles are deposited as low-angle cross-bedding within Bouma division C. The major components in the basal sands cutting into the claystone are volcanic fragments and ooids containing volcanic fragments in their cores. The volcanic fragments are commonly concentrated on the underside of each cross-lamination and enhance the appearance of the sedimentary structure. (Plane polarized light; bar scale = 2.0 mm.) C. Photomicrograph of same sample shown in 10B. (Plane polarized light. Bar scale = 0.5 mm.)

Gregor, et al., 1973b), indicating that this seamount was at or near sea level when the sediments were deposited. We envision a similar setting for the source of shallow-water carbonate clasts preserved in Unit VI.

Many turbidites in the uppermost part of Unit VI are composed primarily of carbonate material; the carbonate sands are interlayered with dominantly volcanogenic and mixed carbonate and volcanogenic turbidites. The proportion of carbonate turbidites is greatest toward the top of the unit, suggesting that the supply of volcano-

genic material decreased while the supply of shallow-water carbonate material increased. At the same time carbonate material derived from pelagic sources became more important. The carbonate debris in the lower part of this unit contains rudist and algal fragments typically associated with reefal environments. In the upper part of this unit, these fragments are noticeably lacking (see discussion in Site 585 report, this volume).

In the overlying Unit V, the sedimentation rate decreases to about 5 m/m.y. (Fig. 17). The primary lithol-

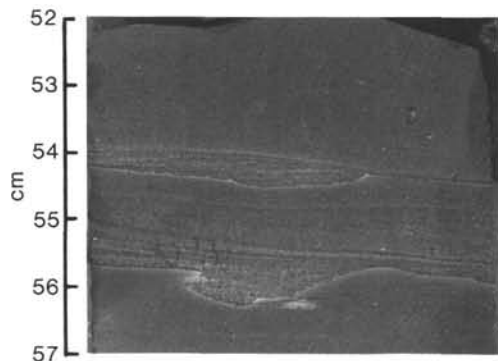


Figure 11. Load casts in sandstone bases of volcanogenic turbidites (585-43-4, 52-57 cm, Unit VI) overlying claystone tops of other turbidites (at 54 and 56 cm).



Figure 12. Well-developed load cast (at 124 cm) formed at boundary between overlying volcanogenic sandstone and underlying claystone (585A-13-1, 122-127 cm, Unit VI).

ologies in this unit are middle Albian to Campanian claystones containing varying proportions of zeolites, carbonate material, and radiolarian sandstones. Graded sequences contain radiolarians as the coarse component. However, no shallow-water carbonate debris was recovered in this unit and there is a marked decrease in the proportion of volcanic debris.

The black layers recovered near the Cenomanian/Turonian boundary in Subunit VB yield organic carbon values close to 10%. The pyritized organic debris in these layers is composed of single-celled marine algae and dinoflagellates (see the section on Organic Geochemistry, Site 585 report, this volume), which implies that the material was produced in the oceanic photic zone.

Several Cretaceous intervals are noted for the widespread occurrence of organic carbon-rich sediments. These layers have been found worldwide in association with the Cenomanian/Turonian boundary, both on land and in the major ocean basins (Schlanger and Jenkyns, 1976; Thiede and van Andel, 1977; Arthur and Schlanger, 1979; Jenkyns, 1980; Schlanger and Cita, 1982; and Dean et al., 1984). The occurrence of these layers is indicative of an anoxic environment. The recovery of anoxic sediments from a variety of open-ocean settings (plateaus, seamounts, and continental margins), as well as from smaller restricted basins, suggests that the cause of the anoxic conditions was global in nature (Schlanger and Jenkyns, 1976). Schlanger and Jenkyns (1976) proposed that the Cretaceous was marked by the development of expanded oxygen minimum zones that spanned depths from

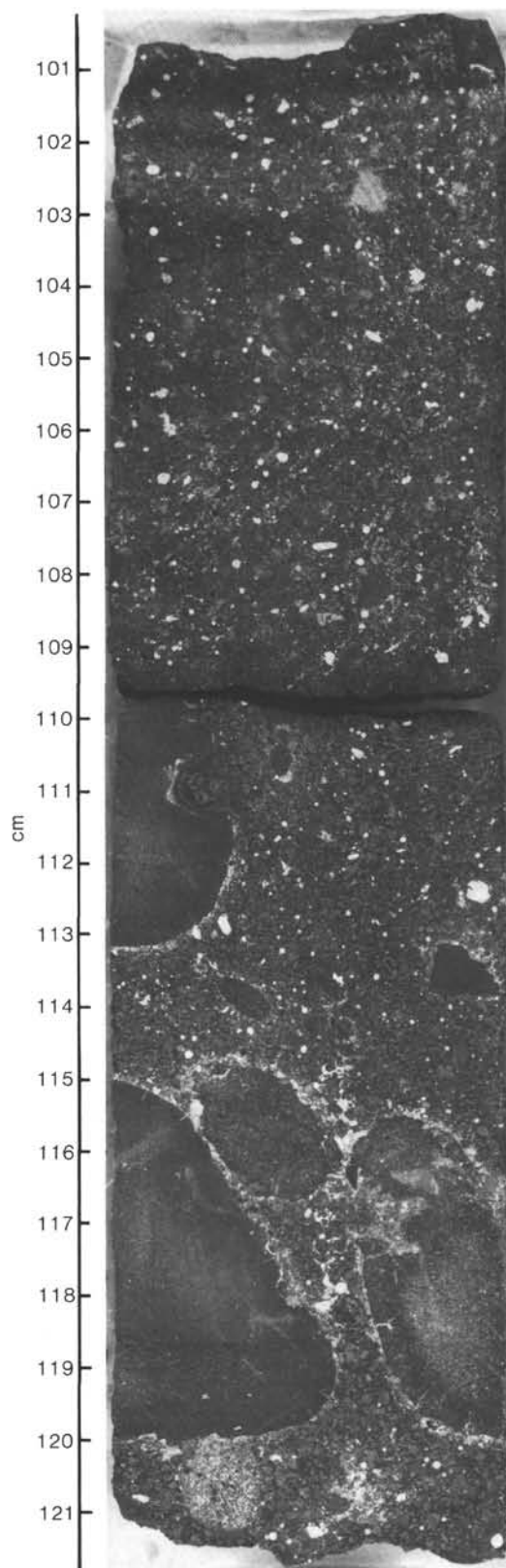


Figure 13. Coarse sandstone from debris flows of Unit VI, recovered near bottom of hole (585A-18,CC). Large (up to 5 cm) rounded basalt clasts are present, with sand-sized grains of hyaloclastic debris, claystone, and abundant shallow-water carbonate debris. Ooids are distinguished by their light color and perfectly round shape. Note the white zeolitic cement rims around many of the grains.

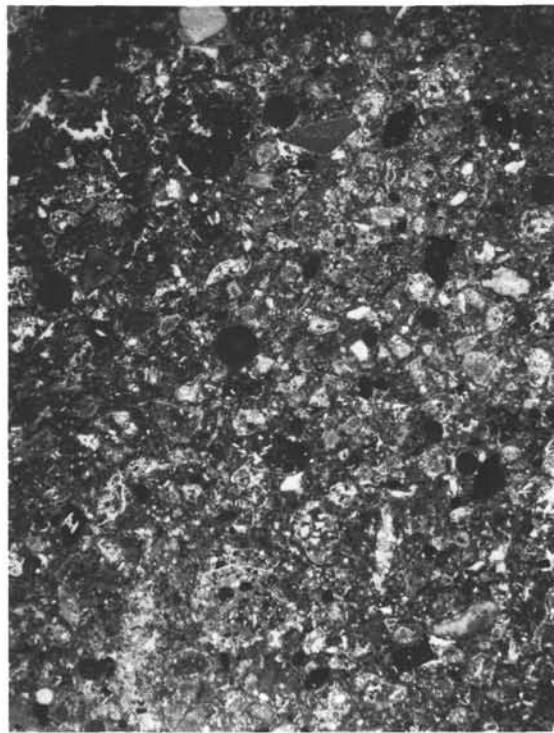


Figure 14. Photomicrograph of Sample 585A-19-3, 15-18 cm. The carbonate debris (ooids, oncoids, abraded mollusk fragments, and an orbitolinid) appears to be floating in the volcaniclastic components of the turbidite deposit. (Plane polarized light; bar scale = 2.0 mm.)

300 to 3000 m. The oxygen minimum zone resulted from a global transgression leading to the increased production of organic carbon in the ocean and a synchronous global warming trend that combined to produce a decrease in the renewal of oxygen in bottom waters.

Concentrations of carbonaceous material were found at the base of graded sequences, and the concentrations decrease upward. The association of these carbonaceous materials with turbidites suggests that the material was reworked and redeposited. Two scenarios are possible: In the first, organic material was initially deposited through pelagic settling into an anoxic basin; the material was then disrupted by a subsequent turbidity current and incorporated into the base of the turbidite, but it was not displaced appreciably from the original site of deposition. Alternatively, the organic material was initially deposited at a shallower depth (e.g., on the flank of a seamount within an anoxic zone of the water column); after deposition, the material was eroded, transported into the basin and redeposited at the base of a graded sequence.

We favor the second scenario. It is unlikely that the oxygen minimum zone extended to the floor of a basin that was already quite deep (>5000 m, see later discussion). No organic carbon-rich or anoxic pelagic division E was found near the Cenomanian/Turonian part of the section or anywhere else at Site 585. The sedimentary structures (graded bedding, cross-laminae, etc.) suggest that the organic debris was transported and deposited with other material in a turbidity current. If the oxygen minimum zone extended from 300 to 3000 m (Schlanger

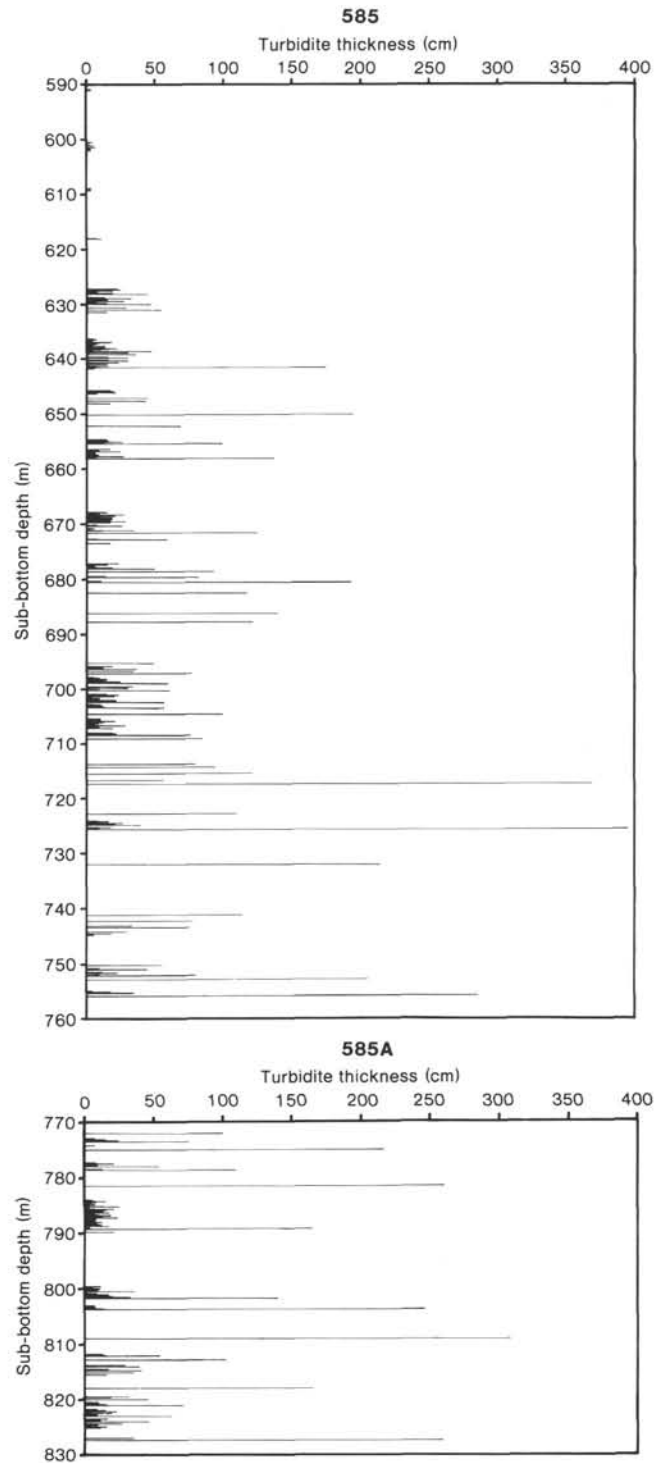


Figure 15. Thicknesses of individual turbidites in Unit VI plotted against sub-bottom depth.

and Jenkyns, 1976), the reduced layer must have been deposited initially between these depths. It is also likely that the organic carbon was pyritized within the anoxic zone and transported after pyritization, producing denser grains of hydraulic equivalence to the silt-sized clasts with which it occurs.

Units I through IV contain pelagic claystones with varying proportions of siliceous and carbonate material.

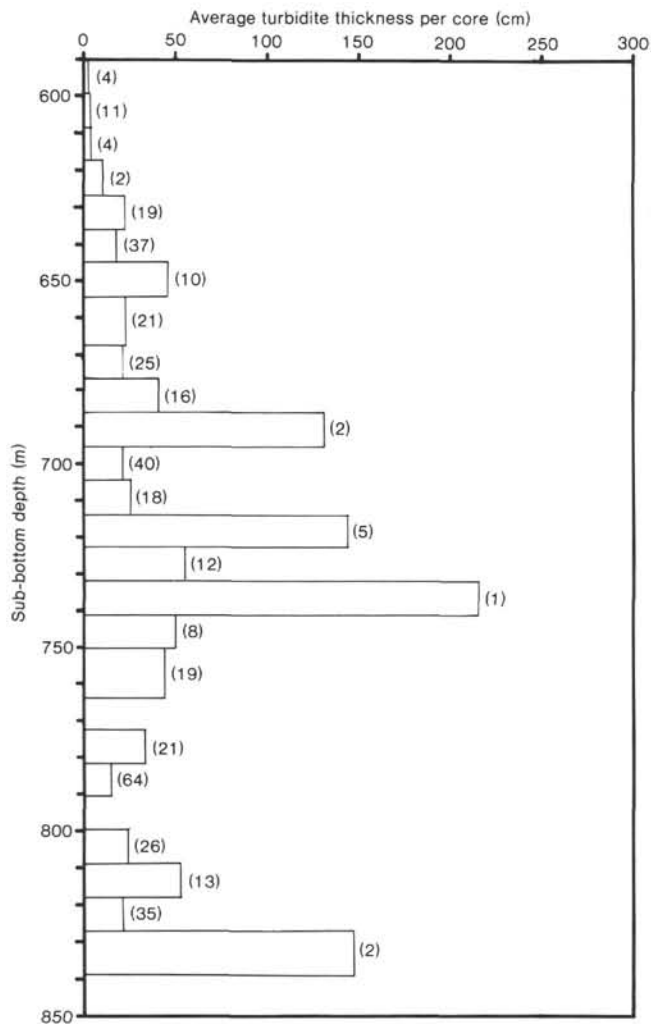


Figure 16. Average turbidite thickness of recovered material in core plotted against sub-bottom depth for Unit VI. Number in parenthesis represents number of turbidites in each core over which the average was calculated.

Graded sequences are apparent in Units III and IV, indicating that turbidity currents were still active. In Units I and II, the presence of carbonate-rich sediments in a basin well below the CCD suggests continued transport and redeposition of material even in the youngest sediments recovered. Sedimentation rates (Fig. 17) are lower in these units (5–10 m/m.y.), indicating that the rate of supply of material to the Basin was still significantly lower than during the deposition of Unit VI.

The sediments at Site 585 document the evolution of the volcanic edifices surrounding the Basin. The lowermost sediments record a growth phase of the seamounts. By the Aptian, the seamounts must have been at or above sea level. During the Aptian and Albian, turbidity currents transported hyaloclastic debris and shallow-water carbonate debris derived from the tops of the seamounts into the Basin. The decrease in reef-associated fauna up-section suggests that the source environment evolved from a reef-dominated system to a carbonate platform without reefs. These sediments represent the Constructive and Emergent Phases of Kelts and Arthur (1981). The initial

Table 2. Lengths of turbidites cored in Unit VI.

Core	Sub-bottom depth at top of core (m)	Length of core (cm)	Turbidite length in core (cm)			Number of turbidites in core
			Longest	Shortest	Average	
Hole 585						
38	590.4	70	5	2	3.2	4
39	599.5	233	7	3	3.7	11
40	608.7	65	4	3	3.7	4
41	617.8	32	12	9	10.5	2
42	627.0	471	55	3	22.1	19
43	636.1	698	175	2	18.0	37
44	645.3	742	195	8	45.8	10
45	654.4	482	138	4	22.8	21
46	667.8	579	125	2	20.8	25
47	676.9	662	193	3	40.7	16
48	686.1	320	140	122	131.0	2
49	695.2	863	77	3	21.1	40
50	704.4	535	100	4	25.8	18
51	713.5	730	369	56	144.0	5
52	722.7	662	395	3	55.3	12
53	731.8	288	215	215	215.0	1
54	741.0	365	114	3	44.9	8
55	750.1	830	285	2	44.2	19
Hole 585A						
11	772.1	690	215	2	32.9	21
12	781.3	999	260	2	14.7	64
13	790.4	640	246	2	24.6	26
14	808.7	707	308	9	53.3	13
15	817.9	759	165	2	20.9	35
16	827.0	691	258	35	146.5	2

growth of the seamounts must have occurred prior to the Aptian, but material attributed to this phase was not recovered at Site 585.

The sediments above Unit VI record the Subsidence Phase (Kelts and Arthur, 1981) of the seamounts. As they progressively subsided, volcanogenic sediments were no longer produced in significant amounts. Pelagic constituents were deposited on the top and flanks of the seamounts and also redistributed into the Basin by turbidity currents. The contribution of siliceous material decreased and carbonate turbidites became dominant through time. The normal background sedimentation of the Basin, however, consisted of pelagic clay.

HISTORY OF THE BASIN

Site 199 was drilled previously in the Mariana Basin, 70 km to the west of Site 585. The stratigraphy of the upper 900 m of section in the Basin is derived from the drilling results of both sites, combined with seismic reflection data.

Based on extrapolation of spreading rates from the Mesozoic magnetic anomalies in the western Pacific, the age of the crust at Site 585 was interpreted to be 170 m.y. (Shipley et al., 1983; see Fig. 18). Paleomagnetic data from Site 585 indicate northward motion of the Pacific Plate since the Aptian (Site 585 report; Ogg, this volume). The lowermost volcanoclastic turbidites give a late Aptian paleolatitude of $15.0^{\circ}\text{S} \pm 4^{\circ}$. The data at this site indicate that the Pacific Plate moved northward rapidly during the Late Cretaceous, 4.5 cm/yr. from the Aptian through the Campanian. This evidence suggests that the site crossed the equator near the end of the Cretaceous, the same timing as suggested by previous authors (Heezen, MacGregor, Foreman, et al., 1973; Lancelot, 1978, Gordon and Cape, 1981; Whitman, 1981).

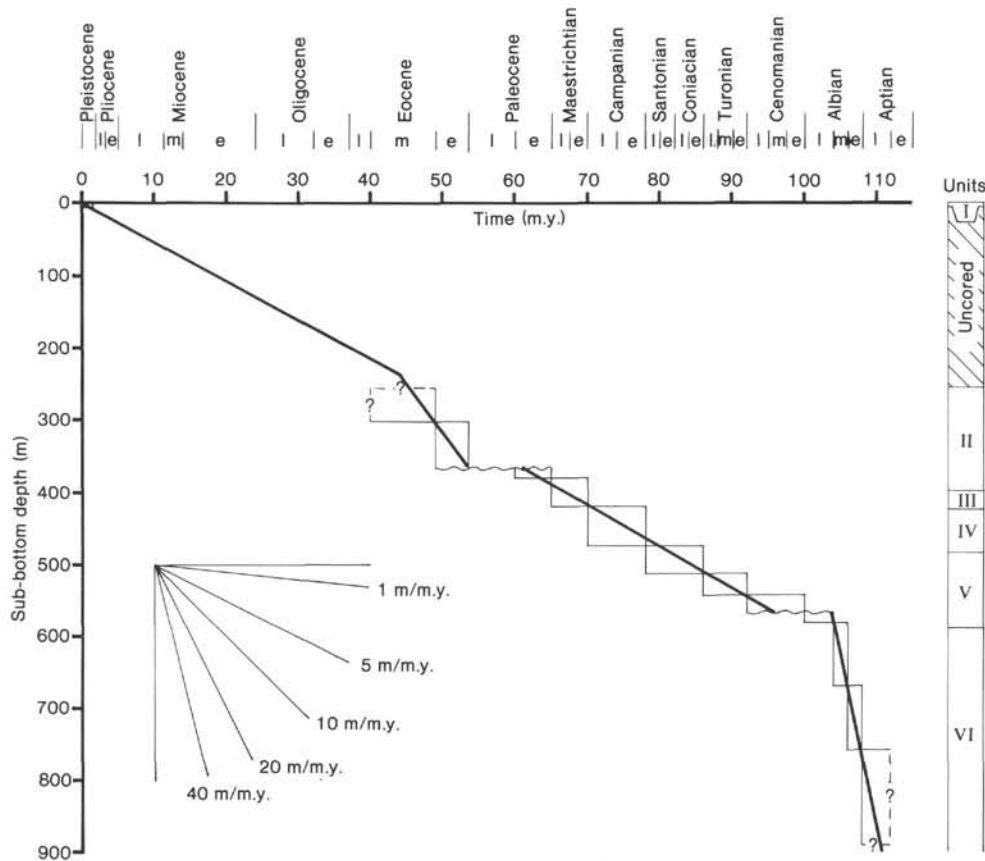


Figure 17. Sedimentation rates for Site 585 (Holes 585 and 585A combined). Sub-bottom intervals of the lithologic units are indicated. Time scale is based on Hardenbohl and Berggren (1978), Berggren and Van Couvering (1974), and van Hinte (1976a, b).

The present latitude of the site is 13.5°N, indicating nearly 35° of northward motion since the late Aptian.

Site 199 was discontinuously cored to a total depth of 456.5 m, with only 13 cores taken. Eight units were identified, labeled A to H from top to bottom (Heezen, MacGregor et al., 1973a). The upper six units (0–275 m) had excellent recovery and are composed of early Pliocene to middle Miocene brown clay, radiolarian ooze, and ash. The upper part of this sequence contains nanofossil turbidites and some graded beds. The lower units (275–456.5 m) had poorer recovery and are characterized by late Paleocene to late Campanian chalk, limestone, chert, and tuff (Fig. 19).

In the interpretation of Heezen, MacGregor, Foreman, et al. (1973), Units G and H are autochthonous products of the site passing beneath the equatorial zone of high productivity during the Late Cretaceous and Paleocene. The chinks and limestones in these units were deposited on seafloor above the CCD. The upper sequence, Units A to F, was deposited on seafloor below the CCD, and the pelagic carbonate material in these units was transported into the Basin by turbidity currents. This model requires either significant seafloor subsidence or a major change in depth of the CCD between deposition of the upper and lower sequences. The tuffs and ash layers that were recovered at the site were interpreted as products of nearby volcanism, particularly during the Late Cretaceous. Based on seismic records, Heezen, Mac-

Gregor, et al. (1973a) estimated that the section contains at least another 200 m of sediment, giving a total thickness of at least 650 m.

Following the drilling of Site 585, the interpretation of the stratigraphy at Site 199 was revised. The section at Site 585 is dominated by material transported by turbidity currents, including the pelagic carbonates that were transported into the Basin from their initial sites of accumulation on nearby seamounts. This process eliminates the need to invoke major changes in subsidence or in the depth of the CCD. The sediments of Units G and H at Site 199 are thus reinterpreted as redeposited material. The increased proportion of biogenic pelagic constituents in the lower sequence at Site 199 is still attributed to the passage of this region beneath the equatorial high productivity zone; however, we believe this material reached the Basin by a two-step process. The northward motion of the region beneath the equatorial zone resulted in an increased accumulation rate of pelagic constituents on the slopes of the seamounts. The sediments were later transported into the deeper areas by turbidity currents. The combined 900-m stratigraphy of Sites 199 and 585 is therefore dominated by redeposited volcanogenic and pelagic debris.

Seismic Stratigraphy

Seismic reflection data were digitally collected in the western Pacific as part of the survey for possible drilling

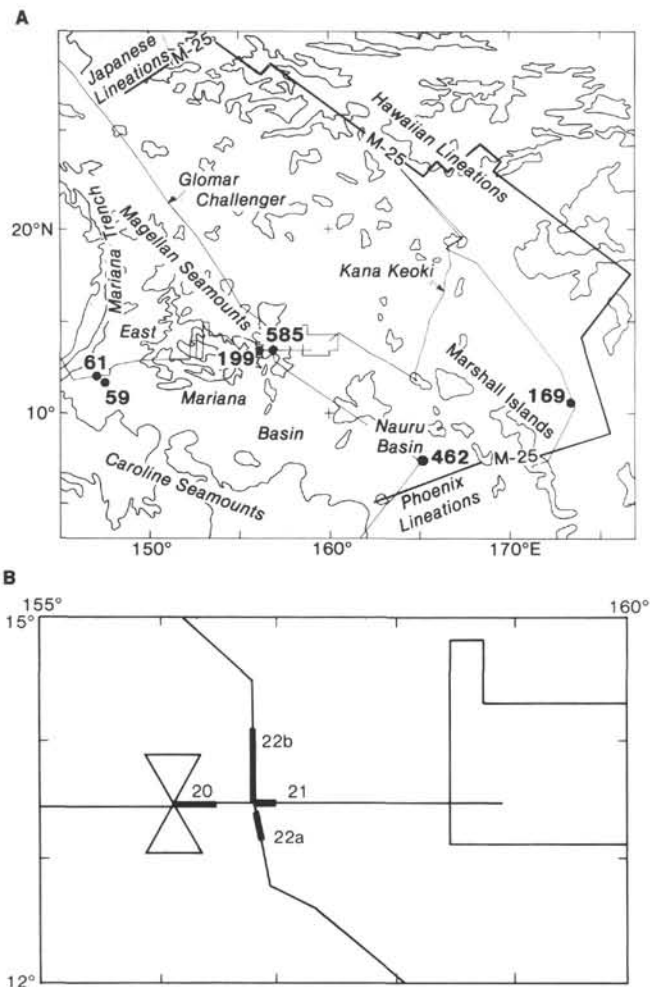


Figure 18. A. Location of Anomaly M-25 (Cande et al., 1978) in the western Pacific (thick line). DSDP sites are shown as dots with site number, and cruise tracks for *Kana Keoki* and *Glomar Challenger* are indicated (thin lines). Bathymetry (after Iwabuchi, 1979) is indicated by 4000- and 6000-m contours; area deeper than 6000 m shaded. Modified from Shipley et al. (1983). B. Blowup of area around Sites 199 and 585. Thick lines and numbers indicate locations of seismic profiles shown in Figures 20, 21, and 22.

sites on old Pacific crust (Petersen et al., this volume; Fig. 18). Two 80-in.³ water guns were employed as a sound source, and sonobuoys were used to determine velocity. An east-west transect was made between Site 199 and the eventual location of Site 585. Seismic reflection data were also digitally collected during Leg 89 of the Deep Sea Drilling Project (Whitman, this volume). The sound source array used on the *Glomar Challenger* consisted of 60- and 120-in.³ air guns. These data provide a north-south transect through the Basin, passing through Site 585 (Fig. 18). The data from the two surveys are combined to describe the three-dimensional stratigraphy within the Basin.

Sonobuoy data in the vicinity of Site 199 gave a 1830 m/s interval from the seafloor to 520 m and a 2010 m/s interval from 520 to 750 m. The underlying highly reflective interval was assumed to have a velocity of 3000 m/s. This model (Shipley et al., 1983) predicted a maximum thickness of the sediment at Site 199 of 1000 m. Figure

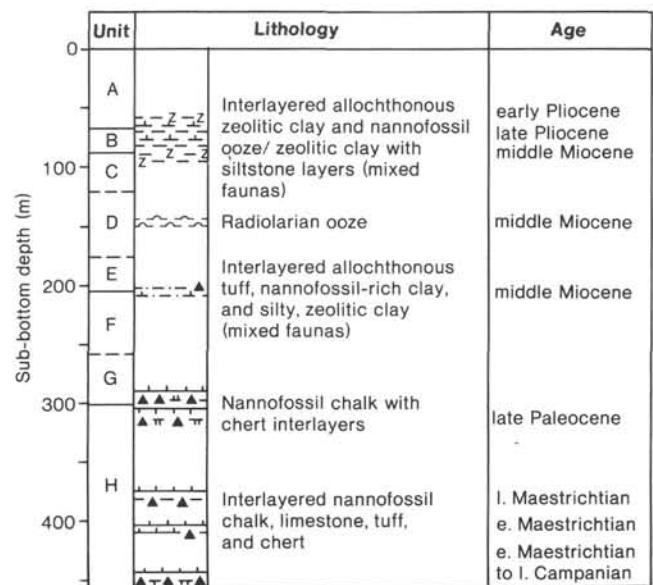


Figure 19. Summary of drilling results at Site 199. Units A-H as labeled by Heezen, MacGregor, et al., 1973a.

20 shows the correlation of these velocity intervals with the seismic and drilling results from Site 199.

The acoustic reflectors at Site 199 can be traced continuously eastward to Site 585 with only slight variations in thickness and sub-bottom depth of the surfaces. Prior to drilling at Site 585, Shipley et al. (1983) predicted the expected stratigraphy at the site. The boundary between the two shallower acoustic units (1830 and 2010 m/s) was traced to 590 m at Hole 585 and the boundary between the two deeper acoustic units (2010 m/s and 3000 m/s) to 890 m, both slightly deeper than at Site 199. This model predicted a stratigraphy based on the initial interpretation of Site 199: turbidites in the upper portion of the section, and pelagic sheet drape dominating the lower portion of the sequence.

With the recovery of the section at Site 585, the interpretation of the seismic stratigraphy in the Basin can be reevaluated (Fig. 21). The sedimentary section at Site 585 is divided into five acoustic units on the basis of compressional sonic velocity and density measurements of the sediments drilled (Units V1 to V5). The boundaries of these units were determined from the lithologic units and seismic profiles as well as from physical properties measurements.

Discontinuous coring and poor recovery make it difficult to distinguish between the upper three acoustic units in the section (Units V1 to V3), which correlate with the upper five lithologic units identified at Site 585 (I-V). Reflectors in this interval (0-590 m sub-bottom), particularly between 8.1 and 8.4 s, are laterally continuous and can be traced across the entire Basin (see also Fig. 22 for a north-south profile through the Basin). This portion of the section is interpreted as fine-grained pelagic turbidites derived from the seamounts surrounding the Basin. These reflectors onlap the seamounts to the north and south of the Basin (Fig. 22). Distinct reflectors at 8.4 and 8.6 s are interpreted as the chert horizons recovered in lithologic Units II and IV.

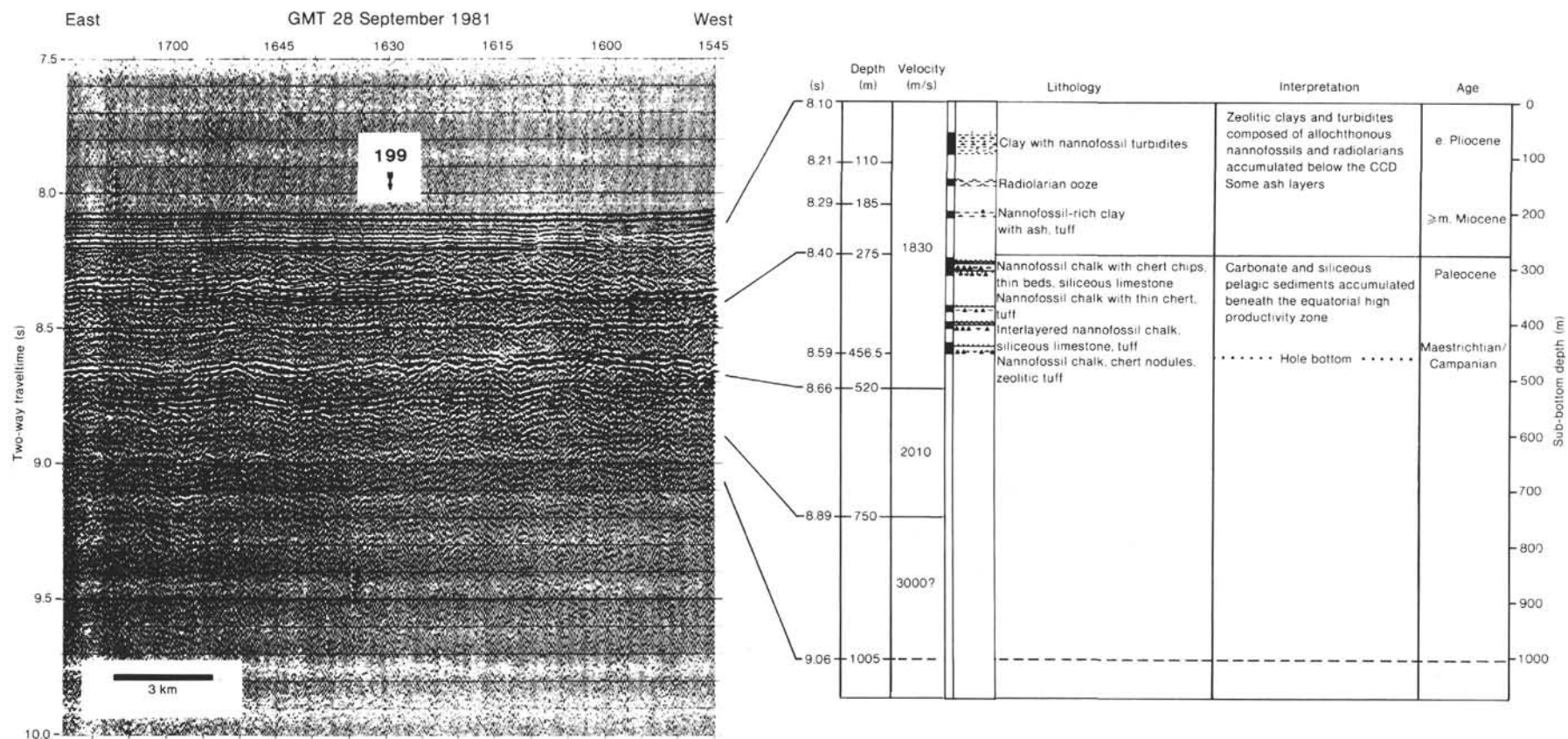


Figure 20. Correlation of Site 199 drilling results, sonobuoy velocity structure, and seismic reflection section (*Kana Keoki* data) in the area of DSDP Site 199 (after Shipley et al., 1983). Section was recorded using two 80-in.³ water guns, bandpass filtered 25–120 Hz. Velocity interval 0 to 530 m (1830 m/s) correlates with basin-leveling sequence (8.10–8.46 s), which thickens toward the center of the Basin and displays onlap at the edges of the Basin and with transitional interval (8.46–8.66 s). Total depth for Site 199 was 456.5 m (8.59 s), which correlates with the base of the transitional interval. Prominent reflectors near 8.4 s (275 m) were interpreted as the bottom of the turbidite sequence at Site 199 (Units A–F), and Units G and H correlate with the transitional interval. The interval from 8.6–9.0 s, containing parallel reflectors that were interpreted as sheet drapes of underlying topography, correlates with the middle velocity interval (2010 m/s; 520–750 m). Lowermost interval (9.0–9.1 s), highly reflective and variable in thickness (50–150 m), is interpreted as covering the high relief top of oceanic basement and correlates with the deepest high velocity interval (3000 m/s).

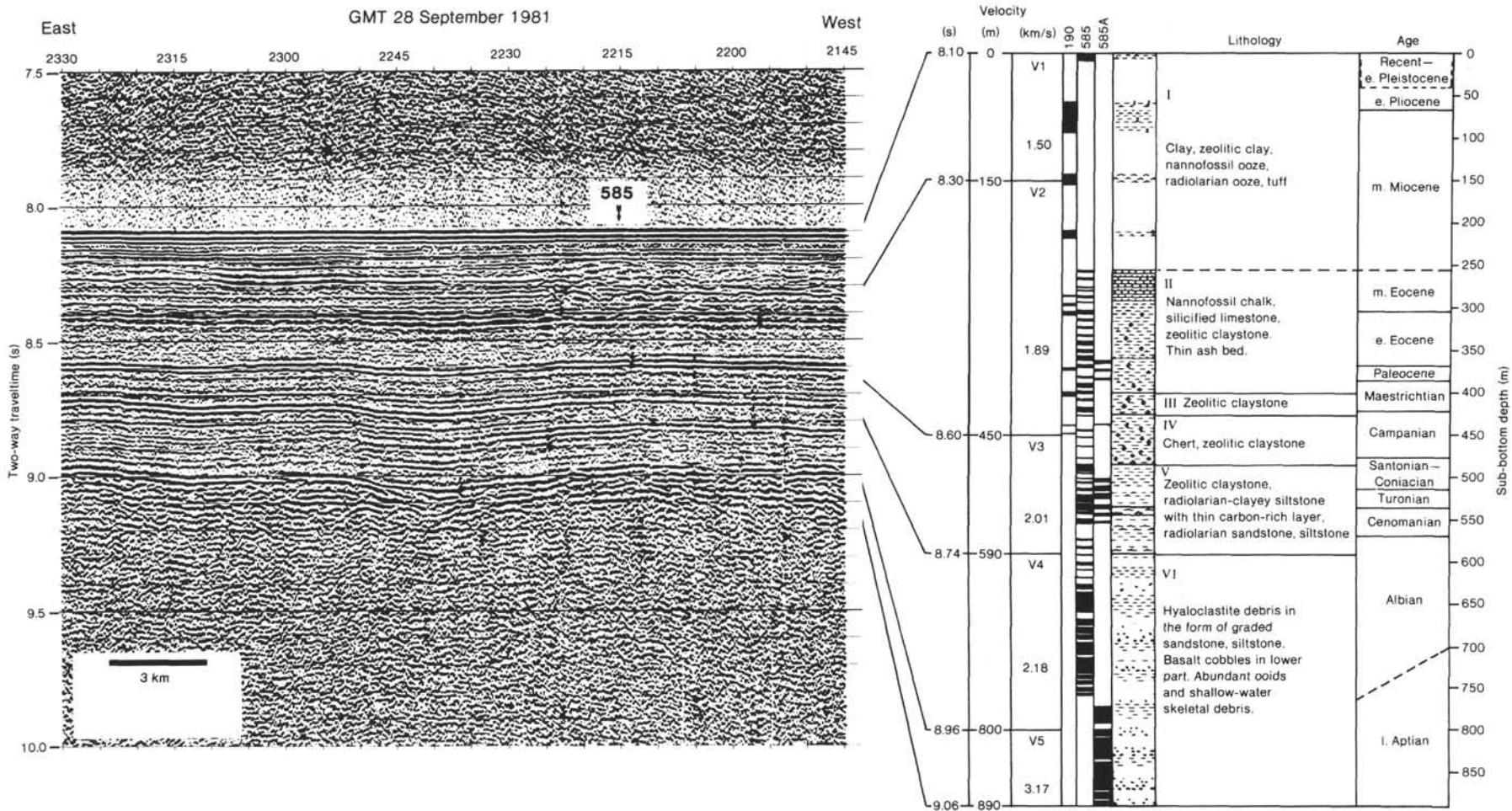
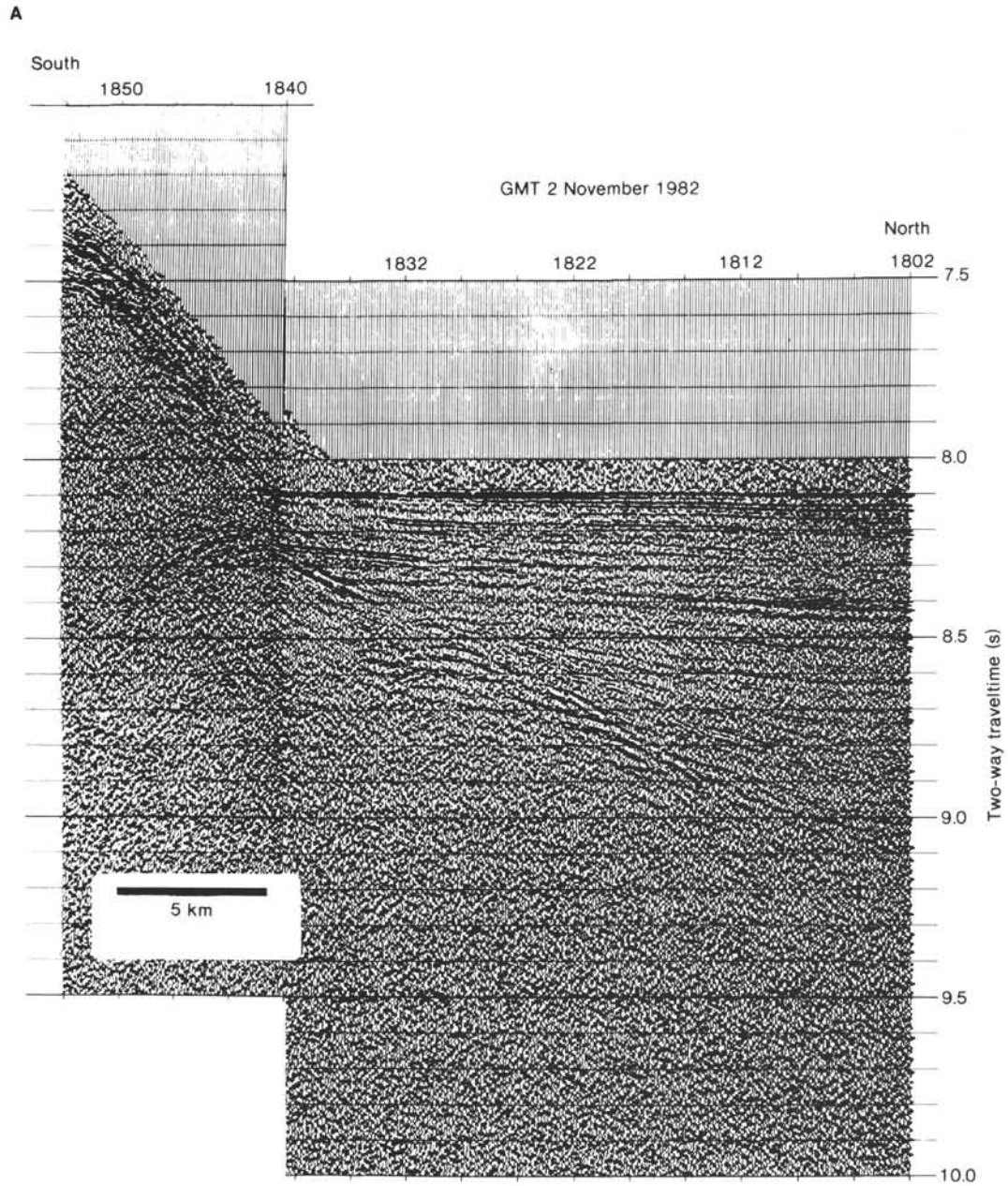


Figure 21. Correlation of drilling results from Sites 199 and 585 with seismic reflection section extending eastward from Site 585 (collected by Kana Keoki). The section was recorded using two 80-in.³ water guns, bandpass filtered 25–120 Hz, AGC window 0.5 s. Acoustic units of Site 585 (V1–V5) and lithologic units based on drilling results of Site 585 (I–VI) are labeled. The depth of the seismic reflectors (s) listed to the right of the profile is the depth at which the reflector occurs beneath Site 585. The tie lines between the stratigraphic column and the seismic section are drawn to the same reflector at the depth where it occurs at the edge of the seismic section.



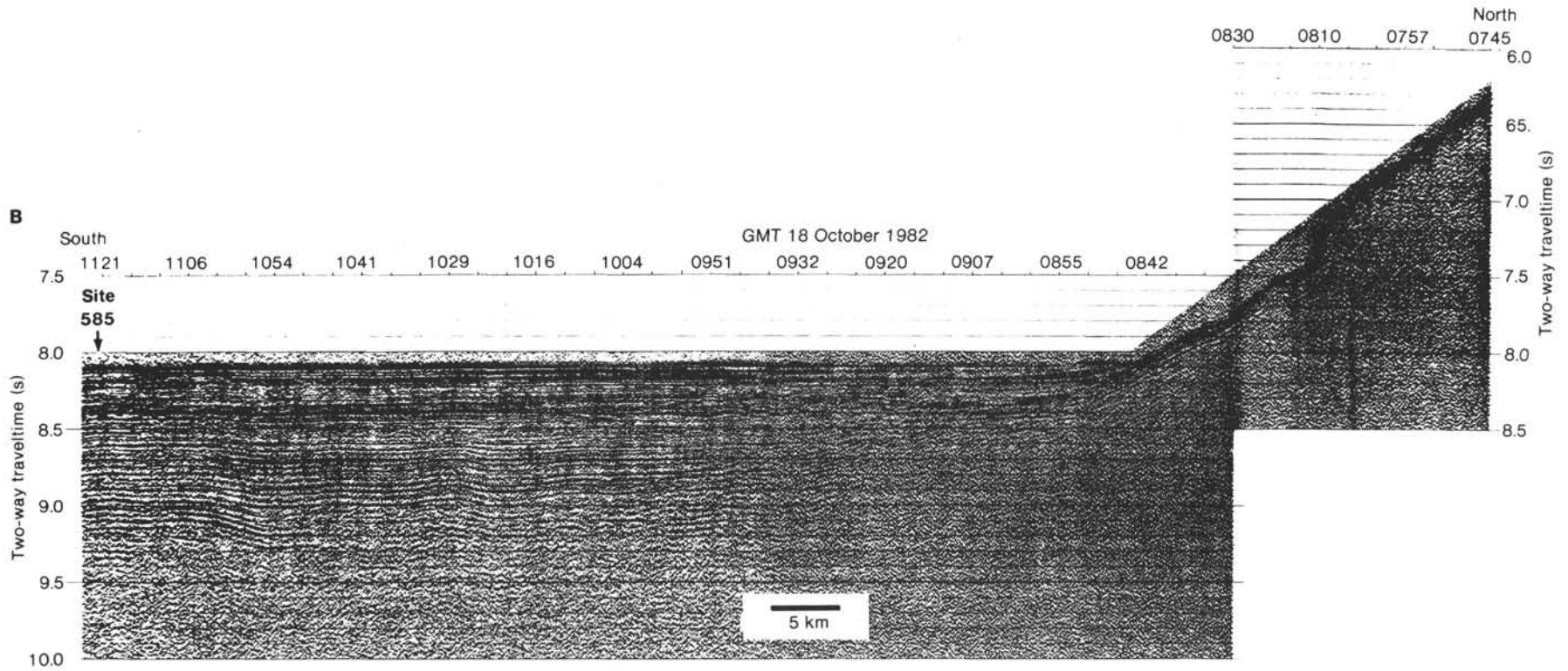


Figure 22. Seismic reflection profiles collected by the *Glomar Challenger* in the Mariana Basin using 120- and 60-in.³ air guns, bandpass filtered 15–100 Hz, AGC window 0.5 s, deconvoluted. A. Section extends northward from slopes of Ita Maitai Guyot toward Site 585. B. Section extends northward from Site 585 to flanks of a seamount. (During Leg 89, a problem with the collection of data at the base of the seamount resulted in loss of penetration.) Note onlap of reflectors on flanks of seamounts in both profiles.

The top of the volcanoclastic sediments at 590 m (the boundary between Units V and VI) correlates with a continuous, high-amplitude reflector at 8.74 s. This reflector also onlaps the volcanic highs around the Basin, and below this reflector, the sedimentary section is composed of coarse-grained turbidites. The major change in lithology is also marked by an increase in acoustic velocity (transition between acoustic Units V3 and V4).

The prominent reflector at 8.96 s is correlated with a marked increase in cementation of the volcanoclastic material at 800 m. This transition is also distinguished by a sharp increase in velocity from 2.2 to 3.2 km/s (the boundary between acoustic Units V4 and V5). Thus the reflector near 9.0 s does not represent basement of Jurassic limestone as originally proposed by Shipley et al. (1983).

Total drilling depth for Site 585 was 893 m, which extrapolates to 9.06 s of two-way traveltime. However, in the region of Site 585, air gun profiles (Fig. 22) indicate that the section extends significantly deeper than drilling penetrated and deeper than the water gun profiles had previously indicated. The reflectors in the lower part of the section (below the top of the volcanoclastics at 8.74 s) are not horizontal. They show structural variation and are less continuous than the reflectors in the upper part of the section; there is also some evidence of filling of local depressions. Penetration in the lower part of the section was not good, but structure is evident to at least 9.2 s at the location of Site 585. Farther to the north (Fig. 22B), the section may extend to at least 9.5 s.

Assuming that igneous basement is not masked by overlying layers, we initially place the base of the sedimentary section at 9.2 s. Extending the lowermost acoustic unit (3.2 km/s) from the reflector at 9.0 s to basement, we calculate a total thickness for the section of 1200 m. If, however, the lowermost acoustic unit extends from 9.0 s to basement at 9.5 s, the total thickness for the section is almost 1700 m. The composition of the section between the total depth of Site 585 and basement is unknown; volcanogenic turbidites may extend deeper than 893 m, but it is unlikely that this material extends all the way to basement because the volcanoes are younger than the crust (see discussion later). Below the volcanogenic material, the sediments may include carbonates that accumulated on the Jurassic ridge crest. Moreover, the acoustic velocity probably continues to increase with depth, which would yield an even thicker section of sediments. In any case, the sedimentary section in this Basin is thicker than earlier predictions indicated (Heezen, MacGregor, et al., 1973a; Shipley et al., 1983).

Subsidence History

Given an initial basement age of 170 m.y., the subsidence history of this area can be recreated by taking into account thermal subsidence and isostatic effect of loading by sediments. Figure 23 shows a subsidence curve for the basement in this region, with the subsidence history of the sedimentary section superimposed. The backtracking of horizons is based on sedimentation rates (Fig. 17), the present thickness and density of the rocks in the

lithologic units, and the age-versus-depth equations of Parsons and Sclater (1977). No corrections were made for changes in compaction through time. This technique yields an estimate of 3110 m for the depth of the Mesozoic ridge crest.

Our predicted ridge crest depth is significantly deeper than present ridge crest depths. This supports 170 m.y., as a minimum age estimate for crust in this region, but it also raises questions about the origin of the crust and its history since formation. If the sedimentary section does extend to 9.5 s, an initial ridge crest depth of almost 3400 m is required. The subsidence history of this basin has been very different from other areas of the oceans, beginning with creation at an anomalously deep spreading center.

Anomalously shallow depths in the Pacific have been attributed to many causes: the thermal effects of widespread midplate volcanism (Schlanger and Premoli Silva, 1981), the emplacement of sills (Larson and Schlanger, 1981), heating of the lithosphere (Schlanger et al., 1981), "asthenospheric bumps" caused by convection cells (Menard, 1973), arches formed because of the load of oceanic volcanoes (Menard, 1964; McNutt and Menard, 1978), and crustal thinning produced by heating from an underlying hotspot (Detrick and Crough, 1978).

Anomalies of excessive depth, however, have received little attention. Moats or peripheral depressions around seamounts have been attributed to the elastic flexure of the lithosphere under the load of volcanoes (Walcott, 1970; McNutt and Menard, 1978). It is possible that this mechanism has affected the Mariana Basin, but the observed anomaly is greater than that generally attributed to moats. Because the Mariana Basin is anomalously deep, it raises the question of whether excessive cooling may have occurred in the area.

Parsons and Sclater (1977) found that the age-versus-depth relationship deviates from a linear square root of age ($t^{1/2}$) model for oceanic crust older than 70 m.y. They proposed that heating at the bottom of the lithosphere maintains a constant plate thickness and causes the subsidence curve to flatten out and approach an asymptotic value for older crust. To resolve this problem, they proposed an exponential relationship between age and depth for crust older than 70 m.y. Our subsidence curve (Fig. 23) uses the two separate equations that they proposed and an isostatic correction for sediment.

Significantly, our calculations for the depth to crust at 170 m.y. falls very close to a $t^{1/2}$ curve. If the crust at this site followed only the linear $t^{1/2}$ relationship, the implication is that the lithosphere did not receive additional heating to maintain a plate of constant thickness; moreover, the plate continued to thicken beyond the maximum value of 125 km suggested by Parsons and Sclater (1977). Pollack et al. (1981) have contoured the thickness of the lithosphere, and the western Pacific is a region of greater thickness than most of the ocean basins. Consequently, we offer the hypothesis that the crust of the Mariana Basin is above a "cold spot"; it received less heat from the mantle, which produced a thickened lithosphere and excess subsidence.

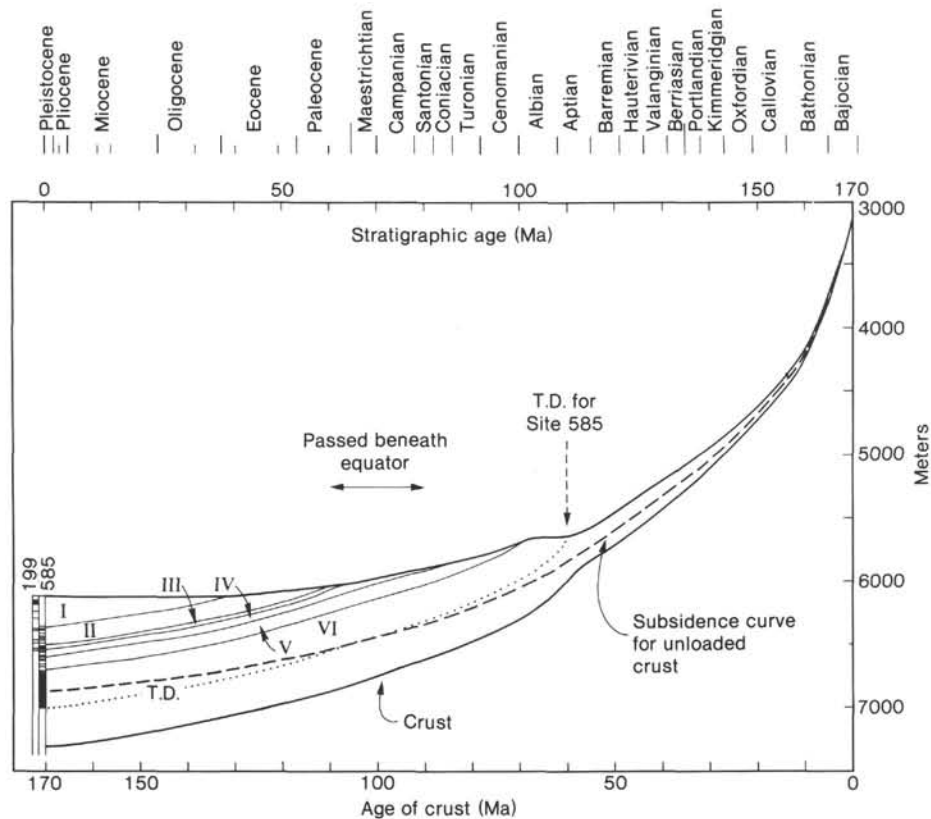


Figure 23. Backtracking curve of the Mariana Basin near Sites 199 and 585. Lithologic units recovered in Site 585 (I–VI), total depth for Site 585 (T.D.), and subsidence curve for 170-m.y.-old unloaded crust are indicated. Thermal subsidence (Parsons and Sclater, 1977) and isostatic correction for sediment loading have been applied. Time scale is based on Hardenbohl and Berggren (1978), Berggren and Van Couvering (1974), and van Hinte (1976a, b).

Mid-Cretaceous Volcanism

The Pacific Ocean basin was the site of extensive mid-plate volcanism during the Late Cretaceous (Menard, 1964; Watts et al., 1980; Schlanger et al., 1981). Evidence for this volcanism comes from the numerous volcanic edifices (Fig. 1) and from volcanogenic sediments that have been cored (Winterer, 1973; Larson, Moberly, et al., 1975; Moberly and Keene, 1975; Cook et al., 1976; Schlanger, Jackson, et al., 1976; Moberly and Jenkyns, 1981; Schlanger and Premoli Silva, 1981). The volcanogenic debris was deposited in turbidites together with shallow-water carbonate debris, indicating that the tops of the volcanic edifices were at or near sea level during this time (Cook et al., 1976; Haggerty et al., 1982; Schlanger and Premoli Silva, 1981).

In the Mariana Basin, the large volume of both redeposited volcanoclastic and carbonate debris and the sedimentary structures of the deposits suggest that there were numerous sources. The recovery of pre-early Tertiary oolite on the top of Ita Maitai Guyot (Heezen et al., 1973b) shows that this seamount was at or near sea level at the time that these sediments were deposited. The top of Ita Maitai is presently at a depth of 1500 m. Using this depth as a minimum estimate for regional subsidence since the middle Cretaceous, we create a hypothetical physiographic map of the Mariana Basin for the late Aptian by simply subtracting 1500 m from existing ba-

thymetry (110 Ma, Fig. 24). The Basin itself has not actually experienced this much subsidence (see curve in Fig. 23), but this model emphasizes the abundance of volcanoes and seamounts that were at or near sea level.

CONCLUSIONS

The sediments at Site 585, combined with those of Site 199, record the history of the Mariana Basin since the Aptian–Albian. The growth of the seamounts surrounding the Basin is recorded in the volcanogenic sands and resedimented shallow-water carbonate debris. The well developed sedimentary structures of this unit indicate transport and deposition by turbidity currents. The sediments in the upper two-thirds of the section reflect the subsidence phase of the seamounts and the accumulation of redeposited pelagic material. Seismic data extend this stratigraphy across the entire Basin, and reflectors onlap the surrounding seamounts.

Assuming that the subsidence history of this Basin has followed an expected path, the 170-m.y.-old crust must have been generated at a ridge crest significantly deeper than modern ridge crests. The thickness of the sediments in this Basin may be as great as 1200–1700 m, indicating an anomalously deep crust for the Basin compared to the rest of the Pacific Ocean basin.

Several events of widespread significance are recorded in the Mariana Basin. The volcanism of the Cretaceous, as deduced from the abundant seamounts of the western

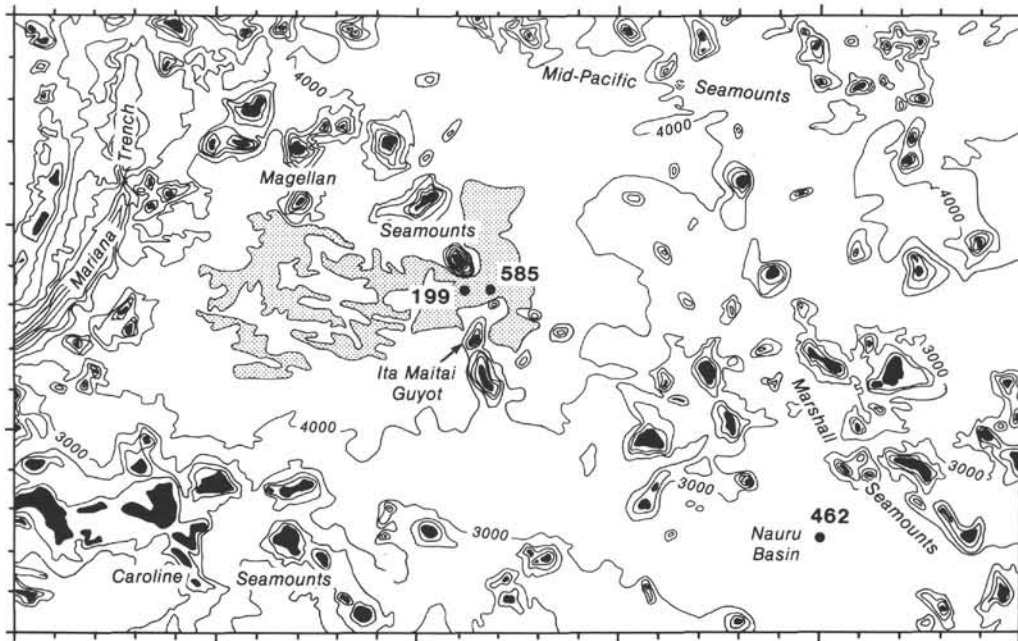


Figure 24. Hypothetical physiographic map of the Mariana Basin and surrounding region in the late Aptian (110 Ma). Areas in solid black are above sea level, the shaded region is the deepest part of the Basin (>4500 m) and contour interval = 1000 m. DSDP sites are indicated by large dots. Latitude and longitude tick marks are at 1° intervals, but no values are assigned, because the Pacific Plate has undergone northward motion and rotation. (See text for further discussion.)

Pacific, is documented in the Mariana Basin; volcanogenic material dominates the Aptian–Albian section and appears throughout the Cretaceous. The growth of mid-Cretaceous reefs in the Pacific and the reworking of shallow-water carbonates are also reflected in the sediments of Site 585. Finally, the oceanic anoxic event at the Cenomanian/Turonian boundary is recorded by the accumulations of partially pyritized organic matter at the bases of turbidites.

ACKNOWLEDGMENTS

We wish to thank reviewers M. B. Underwood, T. H. Shipley, and T. J. Bralower for their efforts and their constructive suggestions. This work was supported by grant IPOD/NSF-C-482 (J.M.W.) and the University of Tulsa Faculty Research Program (J.A.H.).

REFERENCES

Arthur, M. A., and Schlanger, S. O., 1979. Cretaceous "oceanic anoxic events" as causal factors in development of reef-resevoired giant oil fields. *Bull. Am. Assoc. Pet. Geol.*, 63:870–885.

Berger, W. H., and Winterer, E. L., 1974. Plate stratigraphy and the fluctuating carbonate line. In Hsü, K. J., and Jenkyns, H. C. (Eds.), *Pelagic Sediments on Land and Under the Sea*. Int. Assoc. Sedimentol. Spec. Pub. No. 1, pp. 11–48.

Berggren, W. A., and Van Couvering, J. A., 1974. The late Neogene: biostratigraphy, geochronology, and paleoclimatology of the last 15 million years in marine and continental sequences. *Paleogeogr. Paleoclimatol. Paleoecol.*, 16:1–216.

Bouma, A. H., and Hollister, C. D., 1973. Deep ocean basin sedimentation. In Middleton, G. V., and Bouma, A. H. (Eds.), *Turbidites and Deep Water Sedimentation*. Soc. Econ. Paleontol. Mineral. Pacific Section Short Course, pp. 79–118.

Cande, S. C., Larson, R. L., and LaBrecque, J. L., 1978. Magnetic lineations in the Pacific Jurassic quiet zone. *Earth Planet. Sci. Lett.*, 41:434–440.

Chase, T. E., Menard, H. W., and Mammerickx, J., 1970. Bathymetry of the North Pacific. Institute of Marine Resources, Scripps Institution of Oceanography, TR 12.

_____, 1971. Bathymetry of the North Pacific. Institute of Marine Resources, Scripps Institution of Oceanography, TR 11.

Cook, H. E., Jenkyns, H. C., and Kelts, K. R., 1976. Redeposited sediments along the Line Islands, Equatorial Pacific. In Schlanger, S. O., Jackson, E. D., et al., *Init. Repts. DSDP*, 33: Washington (U.S. Govt. Printing Office), 837–847.

Dean, W. E., Claypool, G. E., and Thiede, J., 1984. Accumulation of organic matter in Cretaceous oxygen-deficient depositional environments in the central Pacific Ocean. *Org. Geochem.*, 7:39–51.

Detrick, R. S., and Crough, S. T., 1978. Island subsidence, hot spots and lithospheric thinning. *J. Geophys. Res.* 83:1236–1244.

Gordon, R. G., and Cape, C. D., 1981. Cenozoic latitudinal shift of the Hawaiian hotspot and its implications for true polar wander. *Earth Planet. Sci. Lett.*, 55:37–47.

Haggerty, J. A., Schlanger, S. O., and Premoli Silva, I., 1982. Late Cretaceous and Eocene volcanism in the southern Line Islands and implications for hotspot theory. *Geology*, 10:433–437.

Hardenbohl, J., and Berggren, W. A., 1978. A new Paleogene numerical time scale. In Cohie, G. V., Glassner, M. F., and Hedberg, H. D. (Eds.), *Contributions to the Geologic Time Scale*. Am. Assoc. Pet. Geol. Stud. Geol., 6:213–234.

Heezen, B. C., MacGregor, I. D., and the Shipboard Scientific Party, 1973a. Mesozoic chalks beneath the Caroline abyssal plain; DSDP Site 199. In Heezen, B. C., MacGregor, I. D., et al., *Init. Repts. DSDP*, 20: Washington (U.S. Govt. Printing Office), 65–85.

_____, 1973b. Oolitic limestone on the Ita Mai Guyot, Equatorial Pacific: DSDP Site 202. In Heezen, B. C., MacGregor, I. D., et al., *Init. Repts. DSDP*, 20: Washington (U.S. Govt. Printing Office), 97–102.

Heezen, B. C., MacGregor, I. D., Foreman, H. P., Forristal, G., Hekel, H., Hesse, R., Hoskins, R. H., Jones, E. J. W., Kaneps, A., Krasheninnikov, V. A., Okada, H., and Ruef, M. H., 1973. Diachronous deposits: a kinematic interpretation of the post-Jurassic sedimentary sequence on the Pacific Plate. *Nature*, 241:25–32.

Iwabuchi, Y., 1979. General Bathymetric Chart of the Ocean (sheet 5.06). Canadian Hydrographic Office, Ottawa, Ontario.

Jenkyns, H. C., 1980. Cretaceous anoxic events: from continents to oceans. *J. Geol. Soc. London* 137:171–188.

Kelts, K., and Arthur, M. A., 1981. Turbidites after ten years of Deep Sea Drilling—wringing out the mop? *Soc. Econ. Paleontol. Mineral. Spec. Pub.*, 32:91–127.

- Lancelot, Y., 1978. Relations entre evolution sedimentaire et tectonique de la plaque Pacifique depuis le Cretace Inferieur. *Paris Mem. Soc. Geol. France, Nouvelle Serie No. 134*.
- Larson, R. L., Moberly, R., et al., 1975. *Init. Repts. DSDP*, 32: Washington (U.S. Govt. Printing Office).
- Larson, R. L., and Schlanger, S. O., 1981. Cretaceous volcanism and Jurassic magnetic anomalies in the Nauru Basin, western Pacific Ocean. *Geology*, 9:480-484.
- McNutt, M., and Menard, H. W., 1978. Lithospheric flexure and uplifted atolls. *J. Geophys. Res.*, 83:1206-1212.
- Menard, H. W., 1964. *Marine Geology of the Pacific*: New York (McGraw-Hill).
- , 1973. Depth anomalies and the bobbing of drifting islands. *J. Geophys. Res.*, 78:5128-5137.
- Middleton, G. V., and Hampton, M. A., 1973. Sediment gravity flows: mechanics of flow and deposition. In Middleton, G. V., and Bouma, A. H. (Eds.), *Turbidites and Deep Water Sedimentation*. Soc. Econ. Paleontol. Mineral. Pacific Section Short Course, pp. 1-38.
- Moberly, R., and Jenkyns, H. C., 1981. Cretaceous volcanogenic sediments of the Nauru Basin, Deep Sea Drilling Project Leg 61. In Larson, R. L., Schlanger, S. O., et al., *Init. Repts. DSDP*, 61: Washington (U.S. Govt. Printing Office), 533-548.
- Moberly, R., and Keene, J. B., 1975. Origin and diagenesis of volcanic-rich sediments from North Pacific Seamounts. DSDP Leg 32. In Larson, R. L., Moberly, R., et al., *Init. Repts. DSDP*, 32: Washington (U.S. Govt. Printing Office), 537-546.
- Parsons, B., and Sclater, J. G., 1977. An analysis of the variation of ocean floor bathymetry and heat flow with age. *J. Geophys. Res.*, 82:803-827.
- Pollack, H. N., Gass, I. G., Thorpe, R. S., and Chapman, D. S., 1981. On the vulnerability of lithospheric plates to mid-plate volcanism: reply to comments by P. R. Vogt. *J. Geophys. Res.*, 86: 961-966.
- Schlanger, S. O., and Cita, M. B., 1982. *Nature and Origin of Cretaceous Carbon-Rich Facies*: New York (Academic Press).
- Schlanger, S. O., Jackson, E. D., et al., 1976. *Init. Repts. DSDP*, 33: Washington (U.S. Govt. Printing Office).
- Schlanger, S. O., and Jenkyns, H. C., 1976. Cretaceous oceanic anoxic events: causes and consequences. *Geol. Mijnbouw*, 55:179-184.
- Schlanger, S. O., Jenkyns, H. C., and Premoli Silva, I., 1981. Volcanism and vertical tectonics in the Pacific Basin related to global Cretaceous transgressions. *Earth Planet. Sci. Lett.*, 52:435-449.
- Schlanger, S. O., and Premoli Silva, I., 1981. Tectonic, volcanic, and paleogeographic implications of redeposited reef faunas of Late Cretaceous and Tertiary age from the Nauru Basin and the Line Islands. In Larson, R. L., Schlanger, S. O., et al., *Init. Repts. DSDP*, 61: Washington (U.S. Govt. Printing Office), 817-827.
- Shiple, T. H., Whitman, J. M., Duennebie, F. K., and Petersen, L. D., 1983. Seismic stratigraphy and sedimentation history of the East Mariana Basin, western Pacific. *Earth Planet. Sci. Lett.*, 64: 257-275.
- Thiede, J., and van Andel, T. H., 1977. The paleoenvironment of anaerobic sediments in the late Mesozoic South Atlantic Ocean. *Earth Planet. Sci. Lett.*, 33:301-309.
- van Hinte, J. E., 1976a. A Cretaceous time scale. *Bull. Am. Assoc. Pet. Geol.*, 60:498-516.
- van Hinte, J. E., 1976b. A Jurassic time scale. *Bull. Am. Assoc. Pet. Geol.*, 60:489-497.
- Walcott, R. I., 1970. Flexure of the lithosphere at Hawaii. *Tectonophysics*, 9:435-446.
- Watts, A. B., Bodine, J. H., and Ribe, N. M., 1980. Observations of flexure and the geological evolution of the Pacific Ocean basin. *Nature*, 283:532-537.
- Whitman, J. M., 1981. Tectonic and Bathymetric Evolution of the Pacific Ocean Basin Since 74 Ma [Master's thesis]. University of Miami, Florida.
- Winterer, E. L., 1973. Regional Problems. In Winterer, E. L., Ewing, J. I., et al., *Init. Repts. DSDP*, 17: Washington (U.S. Govt. Printing Office), 911-922.

Date of Initial Receipt: 1 February 1985

Date of Acceptance: 11 April 1985